GPO PRICE $ _____

CFSTI PRICE(S) $ _____

Hard copy (HC) 4.00

Microfiche (MF) .50

ff 653 July 65

FACILITY FORM 602

N66 30188 (ACCESSION NUMBER)	(THRU)
58 (PAGES)	1 (CODE)
CR-76123 (NASA CR OR TMX OR AD NUMBER)	07 (CATEGORY)

JET PROPULSION LABORATORY
CALIFORNIA INSTITUTE OF TECHNOLOGY
PASADENA, CALIFORNIA

897-38529

RE-ORDER No. 64-52

FINAL REPORT FOR

MODIFICATION OF DSIF SCM FEEDS

11 JUNE 1963 - 7 JANUARY 1964

CONTRACT NO. 950639

This work was performed for the Jet Propulsion Laboratory, California Institute of Technology, sponsored by the National Aeronautics and Space Administration under Contract NAS7-100.

Prepared By

HUGHES AIRCRAFT COMPANY
GROUND SYSTEMS GROUP
FULLERTON, CALIFORNIA

FOR

JET PROPULSION LABORATORY
PASADENA, CALIFORNIA

MODIFICATION OF DSIF SCM FEEDS

FINAL REPORT

11 JANUARY 1964

JPL Contract No. 950639

Introduction

The purpose of this program was to study the feasibility and develop a technique for using several modes in a rectangular horn to accomplish primary pattern shaping and monopulse capability for use as a high performance Cassegrain feed. Such a technique was formulated, a design procedure established, and a unit was fabricated and tested. This feed provides monopulse tracking in two planes, dual circular polarization capability, and less than 1° Kelvin noise contribution from interchannel coupling in the monopulse bridge. A discussion of the theory, design, and experimental results of this unit follow.

Theory of Operation

The multimode monopulse horn utilizes the basic TE_{10} mode to provide a reference channel radiation pattern. In addition, the TE_{12}, TM_{12} and TE_{30} modes are used to obtain sidelobe suppression. The field configurations of these modes are shown in Figure 1a. The radiation patterns of these modes in the E and H-planes are shown in Figure 2. The resultant radiation patterns in the two planes indicating sidelobe suppression are also shown.

Monopulse capability is achieved in the same horn by using the TE_{11} and TM_{11} modes to form the E-plane difference pattern and the TE_{20} mode for the H-plane difference pattern. Field configurations of the difference modes are shown in Figure 1b. Also, the theoretical radiation patterns are shown in Figure 3.

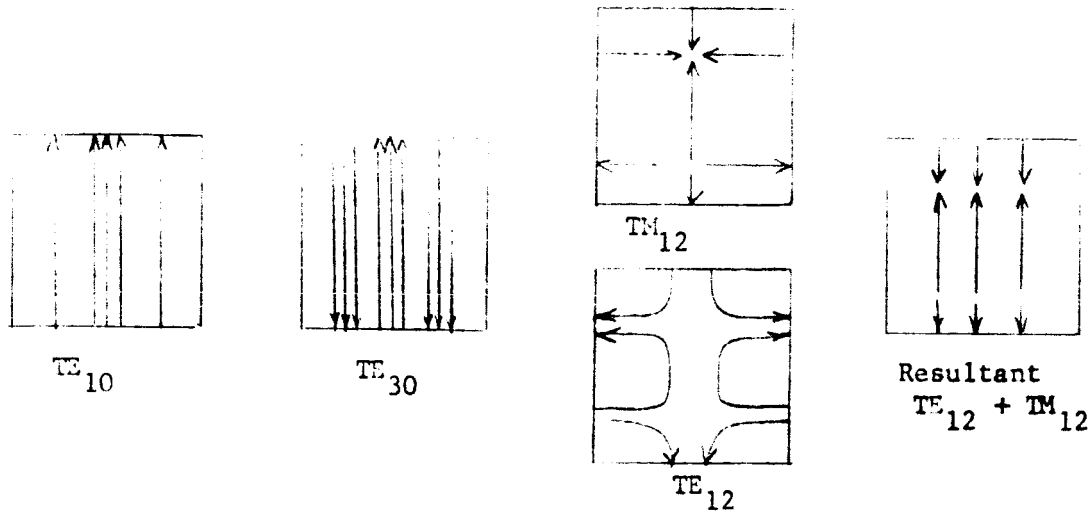

(a) Sum Pattern Modes

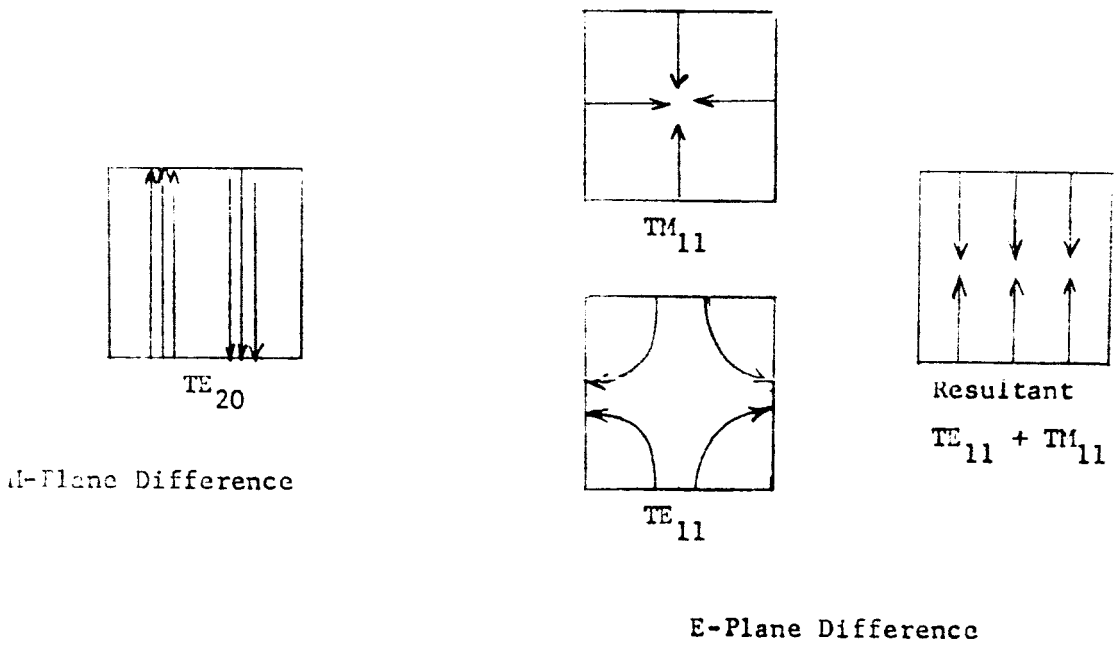

(b) Difference Pattern Modes

Figure 1 Multimode Horn Field Configurations

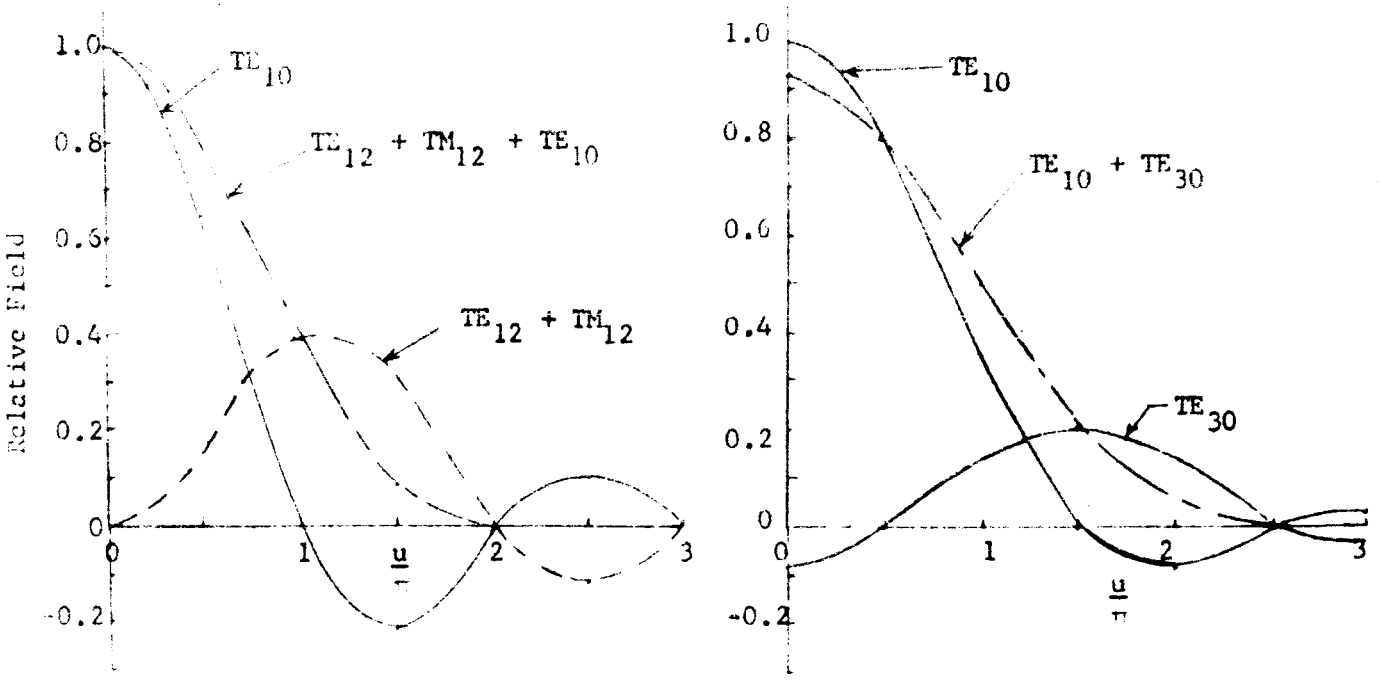

E-Plane Sum Patterns

H-Plane Sum Patterns

Figure 2 Sum Radiation Patterns - Theoretical

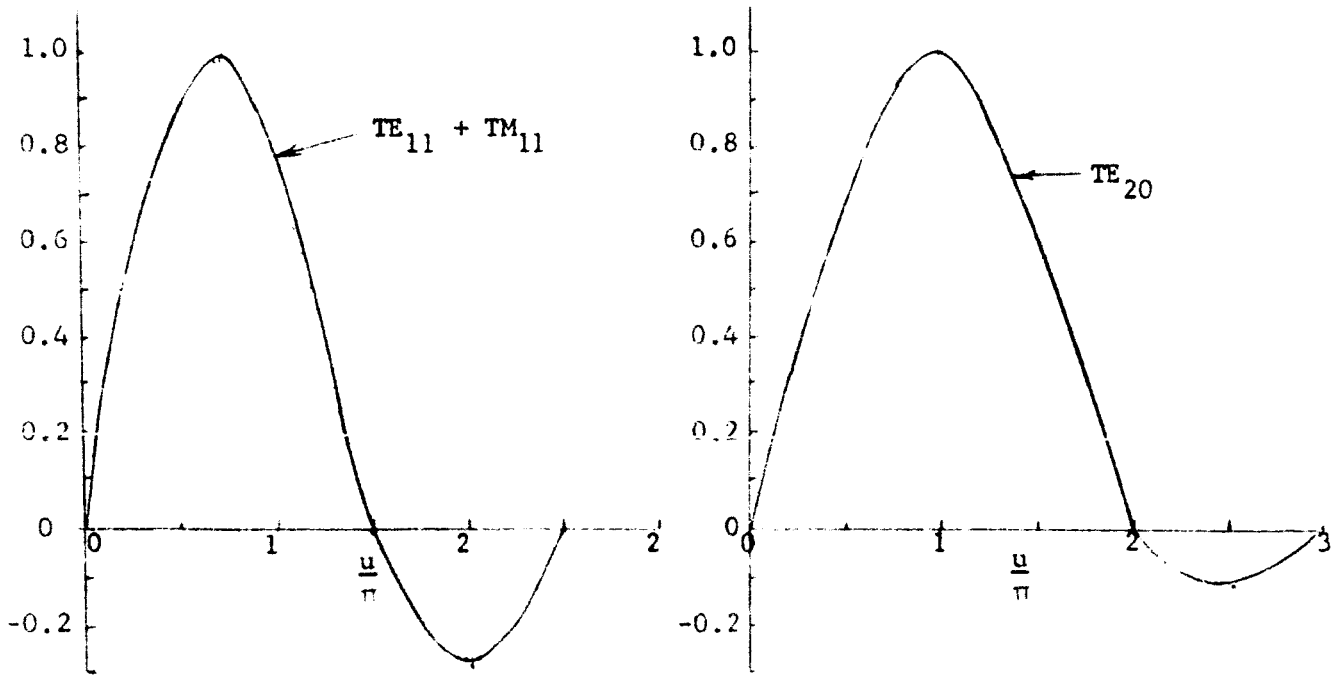

E-Plane Difference Pattern

H-Plane Difference Pattern

Figure 3 Difference Radiation Patterns - Theoretical

RE-ORDER No. 61-3

To result in the desired patterns, the relative phase and amplitude of these modes must be controlled, which is one major design problem. This problem was the main topic of investigation in this study. The second problem is the excitation of the basic modes from the monopulse circuitry and matching these modes into the multimode horn. This has been accomplished experimentally for the sum modes, and over a very limited band for the difference pattern modes.

Mode Generation and Control

A cross section of the multimode horn is shown in Figure 4. The monopulse bridge feeding the common aperture section is a standard four guide monopulse circuit providing dual polarization capability, see Figure 5. The excitation of the multimode section by the four guides is shown in Figure 6. Also, the resulting modes in the multimode matching section are shown.

The matching section provides a match for all modes shown in Figure 6 from the bridge input to the multimode horn. A detail of this section is shown in Figure 7. Along with the basic modes desired, additional higher order modes are excited to meet the boundary conditions. These modes are below cutoff in the matching section, thus causing a large reactive mismatch which must be compensated for by the matching section.

The difference mode phasing section is required to ensure the proper phasing between the TE_{20} and the composite TE_{11} and TM_{11} mode to provide a circularly polarized difference pattern. This is necessary because of the difference in propagation velocity between the modes through the length of the horn. The length of this section is chosen to provide the additional differential phase shift between the modes to result in the correct phase relationship at the aperture.

The sum mode excitation and control section is the most critical portion of the horn. The step between region C and D is chosen such that in addition to the TE_{10} mode, the TE_{12} and TM_{12} and TE_{30} modes are excited from the incident TE_{10} mode with the correct amplitude. The field configurations of these modes were shown in Figure 1. The width "a", of the sum mode control section must be large enough to support all modes up to the TE_{30} mode. It should suppress all higher modes excited by the TE_{11}, TM_{11} and TE_{20} incident modes. It is possible to suppress the TE_{13} and

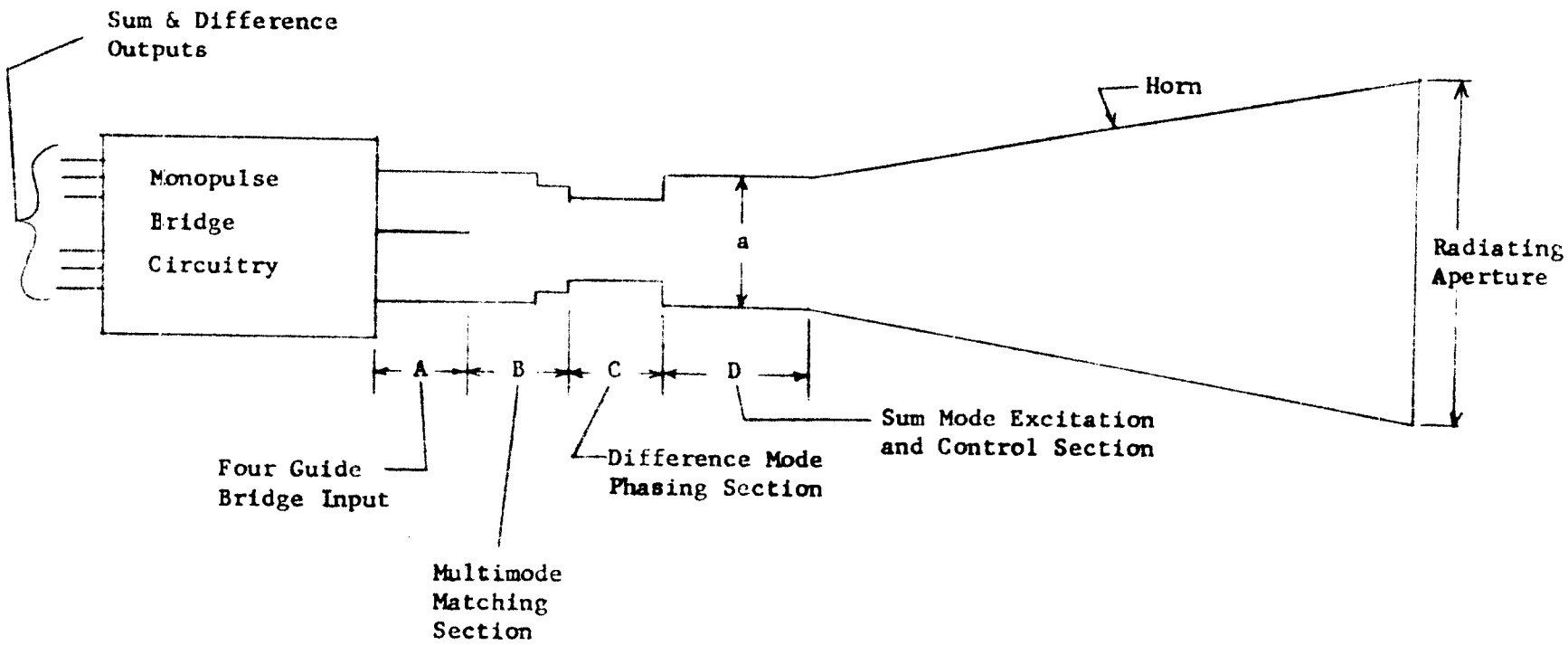

Figure 4 Multimode Feed Cross Section

RF ORDER No. 61-52

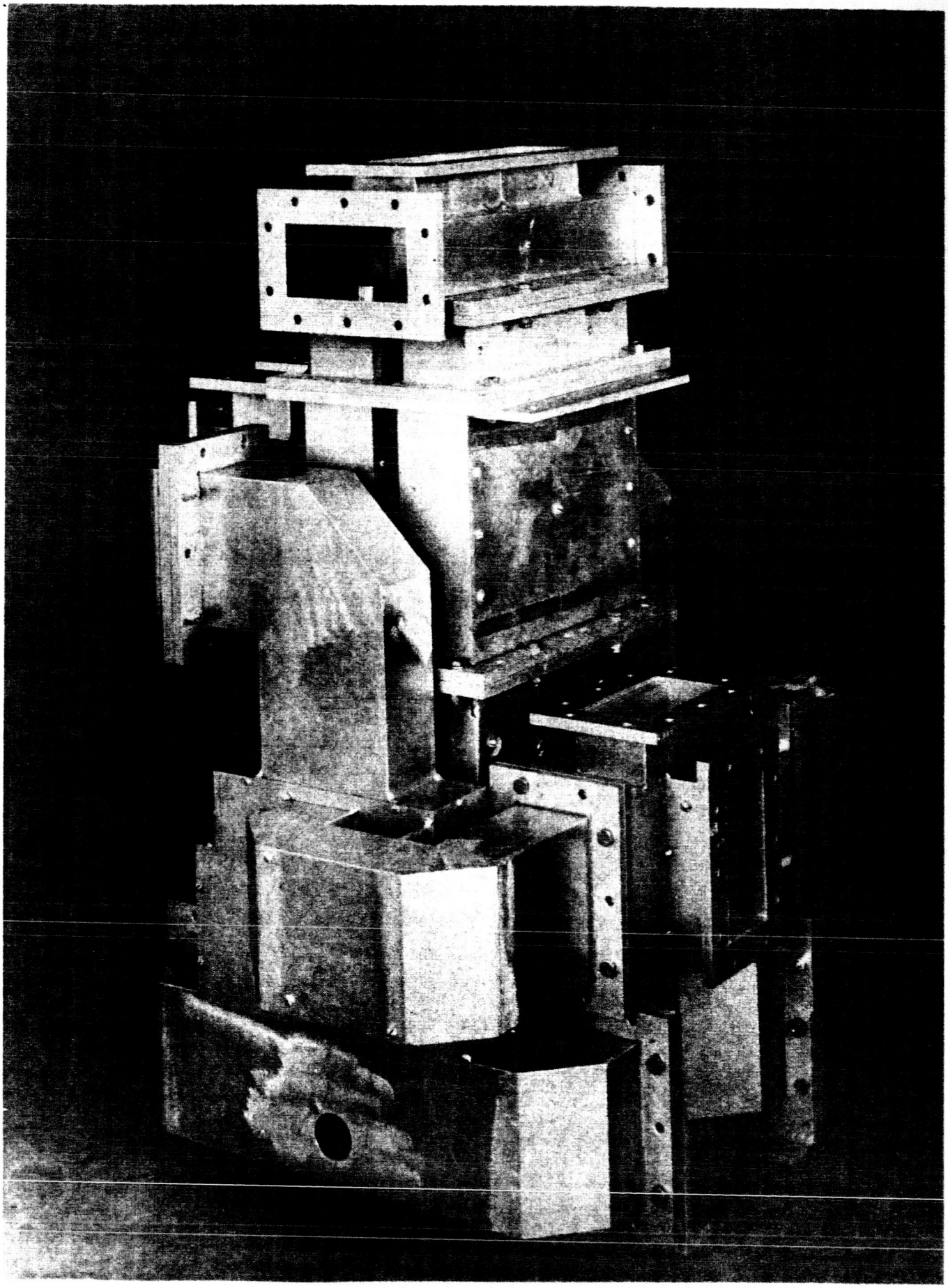

Figure 5 Dual Polarized - Dual Plane Monopulse Bridge Circuitry

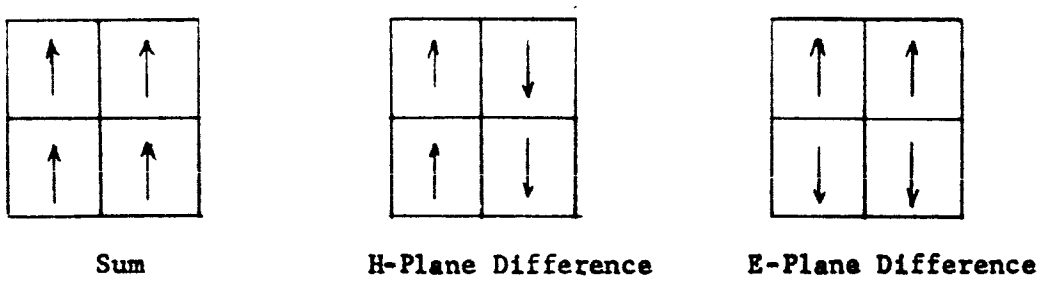

(a) Excitation Field in Four Guide Section

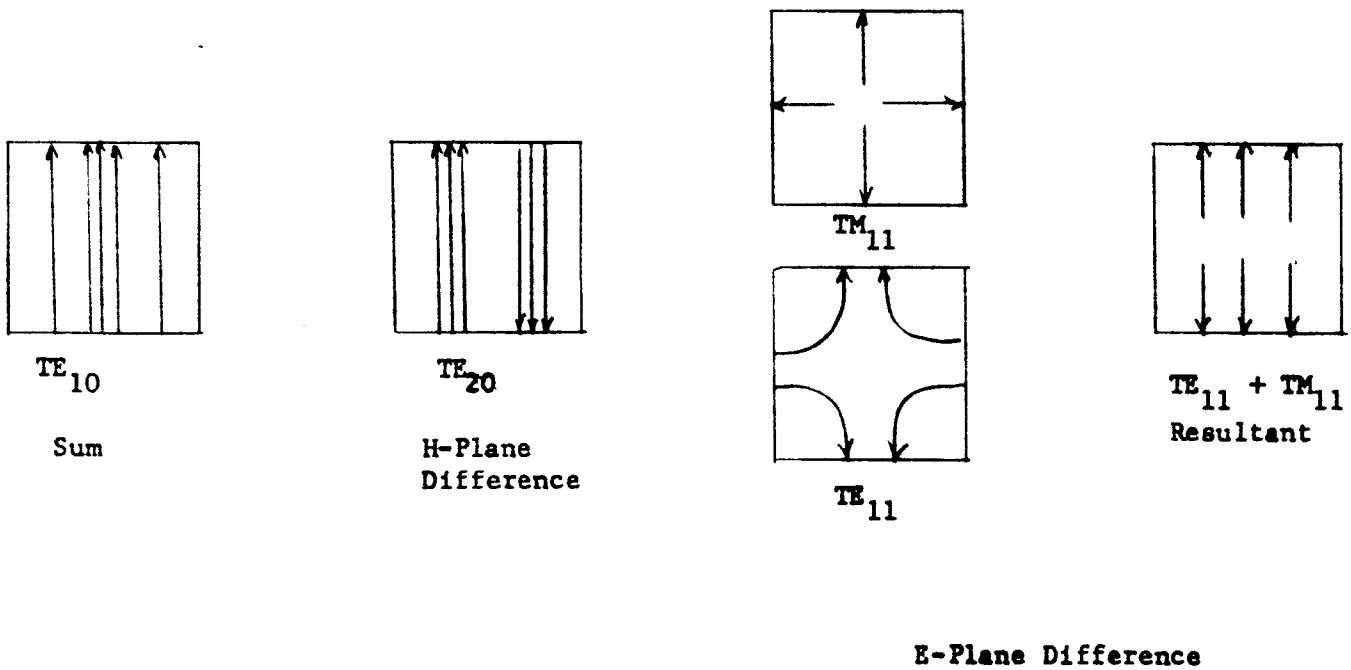

(b) Propagating Modes Excited in Multimode Matching Section

Figure 6 Mode Excitation of Multimode Feed by Monopulse Bridge

RE-ORDER No. 67-522

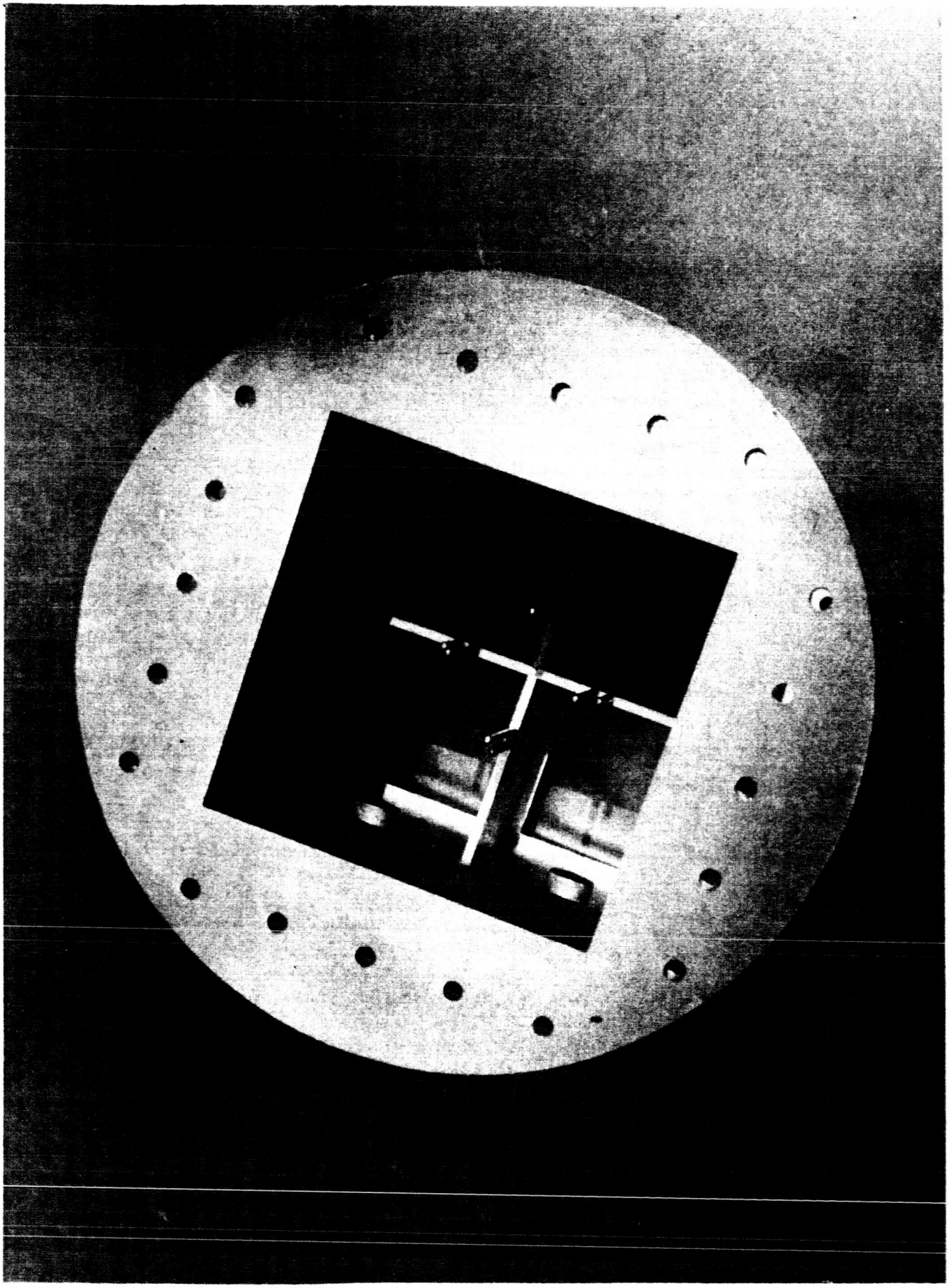

Figure 7 Multimode Matching Section

TM_{13} modes which are excited by the incident TE_{11} and TM_{11} in modes. However, the TE_{22} and TM_{22} modes excited by the incident TE_{20} mode crossing the step have lower cutoff frequencies than the TE_{30} mode and must be allowed to propagate. The effect of this mode combination is to affect the radiation pattern magnitude of the TE_{20} mode which in turn affects the difference pattern axial ratio. Therefore, when phasing the difference modes, the affect of the TE_{22} and TM_{22} modes must be accounted for, which must be done experimentally at the present time.

The length of the sum mode control section must be chosen to provide the correct phasing of the TE_{10}, TE_{30}, TE_{12} and TM_{12} modes at the aperture. As three separate propagation velocities are involved, there is a unique length which must be determined for a given "a" dimension of the control section. This length is also a function of the aperture size "A" and the horn flare angle.

The design of the horn section requires consideration of both the aperture phase error and phasing between the sum pattern modes. The flare angle should be such that the phase error across the aperture is not excessive. However, the choice of the flare angle determines the required horn length for a given aperture and given "a" dimension of control section. Since the phasing between the modes is a function of length, i.e.,

$$\Delta\phi = \int_0^L (\gamma_1 - \gamma_2)\, dz$$

where $\Delta\phi$ is differential phase shift between modes

γ_1 and γ_2 are the propagation constants of modes 1 and 2 respectively

z = length along horn

the flare angle must be chosen carefully to ensure the correct phasing of all the modes at the aperture.

During the study some investigation was made of the excitation coefficients at the steps, and prediction of the resulting patterns from these coefficients. Results of this work has appeared in the monthly reports. However, it was not possible to obtain satisfactory correlation of experimental and theoretical results. This may be due to several factors; however, one large factor appears to be the inability to accurately predict the mode phasing. Although a relatively small

(less than 20°) phase error between the modes may not appreciably affect the sidelobe cancellation, it does affect the required amplitude of the various modes. This was found to be the case in some simple experiments run at the end of the program. Sufficient results are not available to more specifically determine the design procedure at this time, thus a portion of the design remains experimental as was mentioned previously. It appears that carefully controlled experiments must be performed to accurately determine the effect of steps on mode phasing.

Multimode Horn Design Procedure

The basic multimode geometry is shown in Figure 8. The basic consideration in this design is the phasing of the TE_{10}, TE_{12}, TM_{12} and TE_{30} modes at the aperture. This is accomplished by the mode control section "D" as follows.

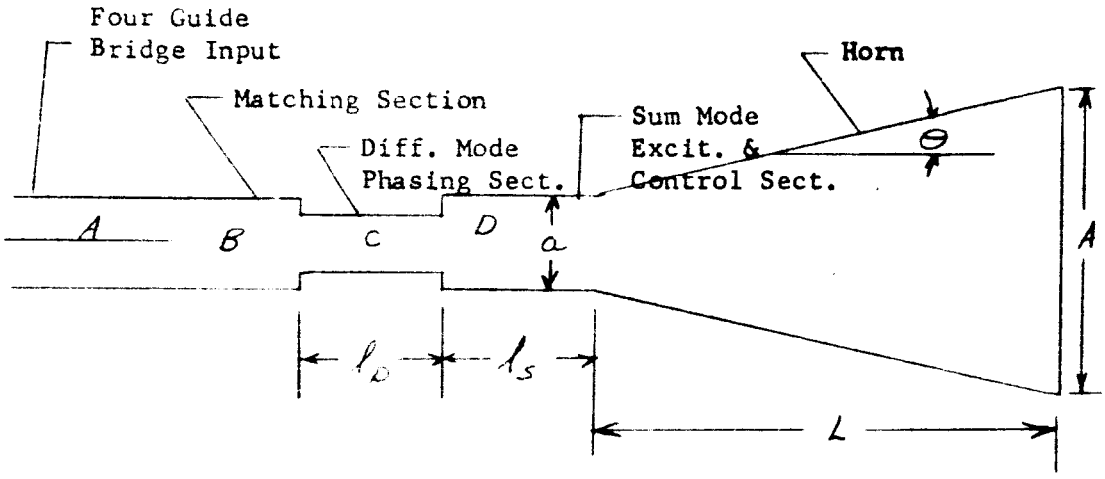

Figure 8

Multimode Horn Geometry

The height "a" and the length "l_s" of the control section (D) is chosen such that the TE_{10} TE_{30}, TE_{12} and TM_{12}, excited in phase at the junction of section (C) and section (D) are again in phase at the aperture. This requires

$$2m\pi = (\beta_{10} - \beta_{30})\, l_s + \Delta\phi_{10-30} \qquad (1)$$

$$2n\pi = (\beta_{10} - \beta_{12})\, l_s + \Delta\phi_{10-12} \qquad (2)$$

where

$\Delta\phi_{10-30}$ = phase between the TE_{10} and TE_{30} after passing thru the horn

$\Delta\phi_{10-12}$ = phase between the TE_{10} and TE_{12} after passing thru the horn

The quantity $\Delta\phi_{10-12}$ is given by the expression

$$\Delta\phi_{10-12} = \int_0^L \left[\beta_{10}(\ell) - \beta_{12}(\ell)\right] d\ell$$

where

$\beta_{10}(\ell)$ = propagation constant of the TE_{10} mode in the horn as a function of " ", etc.

This expression may also be written in terms of the guide size,

$$\Delta\phi_{10-12} = \int_a^A \left[\beta_{10}(a) - \beta_{12}(a)\right] da$$

solving this integral yields the expression

$$\Delta\phi_{10-12}\tan\theta = \frac{\pi}{\lambda}\left\{A\left[\frac{\lambda}{\lambda g_{10}(A)} - \frac{\lambda}{\lambda g_{12}(A)}\right] - a\left[\frac{\lambda}{\lambda g_{10}(a)} - \frac{\lambda}{\lambda g_{12}(a)}\right]\right\}$$

$$+ \frac{\pi}{\lambda}\left\{\frac{1}{P_{10}}\left[\sin^{-1}\frac{\lambda}{\lambda g_{10}(a)} - \sin^{-1}\frac{\lambda}{\lambda g_{10}(A)}\right]\right.$$

$$\left. + \frac{1}{P_{12}}\left[\sin^{-1}\frac{\lambda}{\lambda g_{12}(A)} - \sin^{-1}\frac{\lambda}{\lambda g_{12}(a)}\right]\right\}$$

where: $\frac{\lambda}{\lambda g_{10}(A)}$ is the ratio $\frac{\lambda}{\lambda g}$ for the TE_{10} mode evaluated at "A", etc.

P = the mode cutoff coefficient, $\lambda_c = pa$; $p_{10} = 2$, etc.

This expression must be evaluated for values of $\Delta\phi_{10-12}$ for the particular horn being designed. The similar expression for $\Delta\phi_{10-30}$ must also be evaluated. Detailed calculations may be made to provide design data for typical horn apertures, and as the expression obtained is $\Delta\phi \tan\theta$, the data is valid for horns of any flare angle. For the lower limit on the integral, the dimension of the mode control section "a" must be known, or at least limits on this dimension must be known to provide design data. These limits are set by the requirements

(1) $a > a_{c30}$ i.e., the TE_{30} mode must be able to propagate

(2) $a < a_{c13}$ the TE_{13} and TM_{13} modes, which would be excited by the TE_{11} and TM_{11} modes crossing the discontinuity between sections "C" and "D" must not be allowed to propagate.

This allows limits to be placed on "a", that is:

$$\frac{a_{c30}}{\lambda} < \frac{a}{\lambda} < \frac{a_{c13}}{\lambda}$$

or $$1.5 < \frac{a}{\lambda} < 1.59$$

Graphs #1 and #2 are plots of the function $\Delta\phi_{10-30}\frac{\tan\theta}{\pi}$, and $\Delta\phi_{10-12}\frac{\tan\theta}{\pi}$ for various values of aperture $\frac{"A"}{\lambda}$ and at the limits of $\frac{a}{\lambda}$.

To determine the additional phase shift resulting in the mode control section it is also necessary to know the differential propagation constants in this section

$$\Delta\beta_{10-30} = \beta_{10} - \beta_{30}$$

$$\Delta\beta_{10-12} = \beta_{10} - \beta_{12}$$

and the phase between modes in this section is given by

$$\phi_{c_{10-30}} = (\beta_{10} - \beta_{30})\ell_s = \Delta\beta_{10-30}\ell_s \text{ etc.}$$

The quantities $\Delta\beta_{10-30}$ and $\Delta\beta_{10-12}$ are plotted in Graphs #4 and #5.

The ratio $\frac{\Delta\beta_{10-30}}{\Delta\beta_{10-12}}$ is formed:

$$\frac{\Delta\beta_{10-30}}{\Delta\beta_{10-12}} = \frac{2m\pi - \Delta\phi_{10-30}}{2n\pi - \Delta\phi_{10-12}} \tag{3}$$

When each side of equation (3) is plotted versus $\frac{a}{\lambda}$, the intersection of these two curves determines the value of $\frac{a}{\lambda}$ to result in correct phasing of all sum modes simultaneously. However, before plotting the right hand side of Equation (3), values of m and n must be found to insure a solution. This can be accomplished since $\frac{\Delta\beta_{10-30}}{\Delta\beta_{10-12}}$ has an upper and lower limit determined by the value of $\frac{a}{\lambda}$ large enough to propagate the TE_{30} mode and small enough to cut off the TE_{13} mode. Setting the right hand side of equation (3) first equal to the upper limit and then the lower limit, regions of acceptable $\Delta\phi_{10-30}$ and $\Delta\phi_{10-12}$ are obtained for any given m and n. Alternately, for any given $\Delta\phi_{10-30}$ and $\Delta\phi_{10-12}$, m and n can be chosen to insure a solution. The latter procedure is used in the design since both $\Delta\phi_{10-30}$ and $\Delta\phi_{10-12}$ are slowly varying functions of $\frac{a}{\lambda}$. Graph #5 is a plot of the acceptable region of $\Delta\phi_{10-30}$ and $\Delta\phi_{10-12}$. Values of m and n are given by the integer values of m and n at the apex of the triangular region which includes the point $\Delta\phi_{10-30}$, $\Delta\phi_{10-12}$ for the particular horn being designed.

The value of "ℓ_s" is now determined by using either equation (1) or (2). This completes the design of the sum mode phasing section and horn. The value of "ℓ_D" and the height of the difference modes phasing section (C) is now chosen to bring the TE_{20}, TE_{11} and TM_{11} in phase at the output of the four guide bridge section (A). The height of this section must restrict the TE_{30} and TE_{12} from propagating and allow the TE_{11} and TE_{20} to propagate. The uses of graphs #6, #7 and #8 which show the characteristics of the difference modes will help in determining "ℓ_D" and the height. However, final values must now be determined experimentally. Further investigation of the mode excitation functions in this region may permit a more complete design procedure to be determined.

Summary of the design procedure

(1) Choose $\frac{A}{\lambda}$ (aperture size) and θ (flare angle)

(2) Select a value of $\frac{a}{\lambda}$ which will allow the TE_{30} mode to propagate but not the TE_{13} and determine $\Delta\phi_{10-30}$ and $\Delta\phi_{10-12}$ from Graphs #1 and #2.

(3) Plot $\Delta\phi_{10-30}$ and $\Delta\phi_{10-12}$ on Graph #5 and determine m and n..

(4) Plot $\frac{\Delta\phi_{10-30}}{\Delta\phi_{10-12}}$* and $\frac{2m\pi - \Delta\phi_{10-30}}{2n\pi - \Delta\phi_{10-12}}$ versus $\frac{a}{\lambda}$ using Graphs #1, #2, #3 and #4.

(5) Determine $\frac{a}{\lambda}$ from the intersection on the two curves in step (4)

(6) Calculate "ℓ_s" from either equation (1) or (2).

(7) Determine "ℓ_D" and height of the difference modes phasing section (C) (with the restriction that the TE_{30} and TE_{12} are cut off) to bring the TE_{20} and TE_{11} in phase at the four guide bridge section (A).

*Note: A plot of $\frac{\Delta\phi_{10-30}}{\Delta\phi_{10-12}}$ versus $\frac{a}{\lambda}$ has been included in Graph No. 9 for convenience in solving this step.

The function $\frac{2m\pi - \Delta\phi_{10-30}}{2n\pi - \Delta\phi_{10-12}}$ may be plotted on this same graph to solve Equation 3.

Graph #1

$\Delta\phi_{10-30}\frac{\tan\theta}{\pi}$ vs. $\frac{A}{\lambda}$

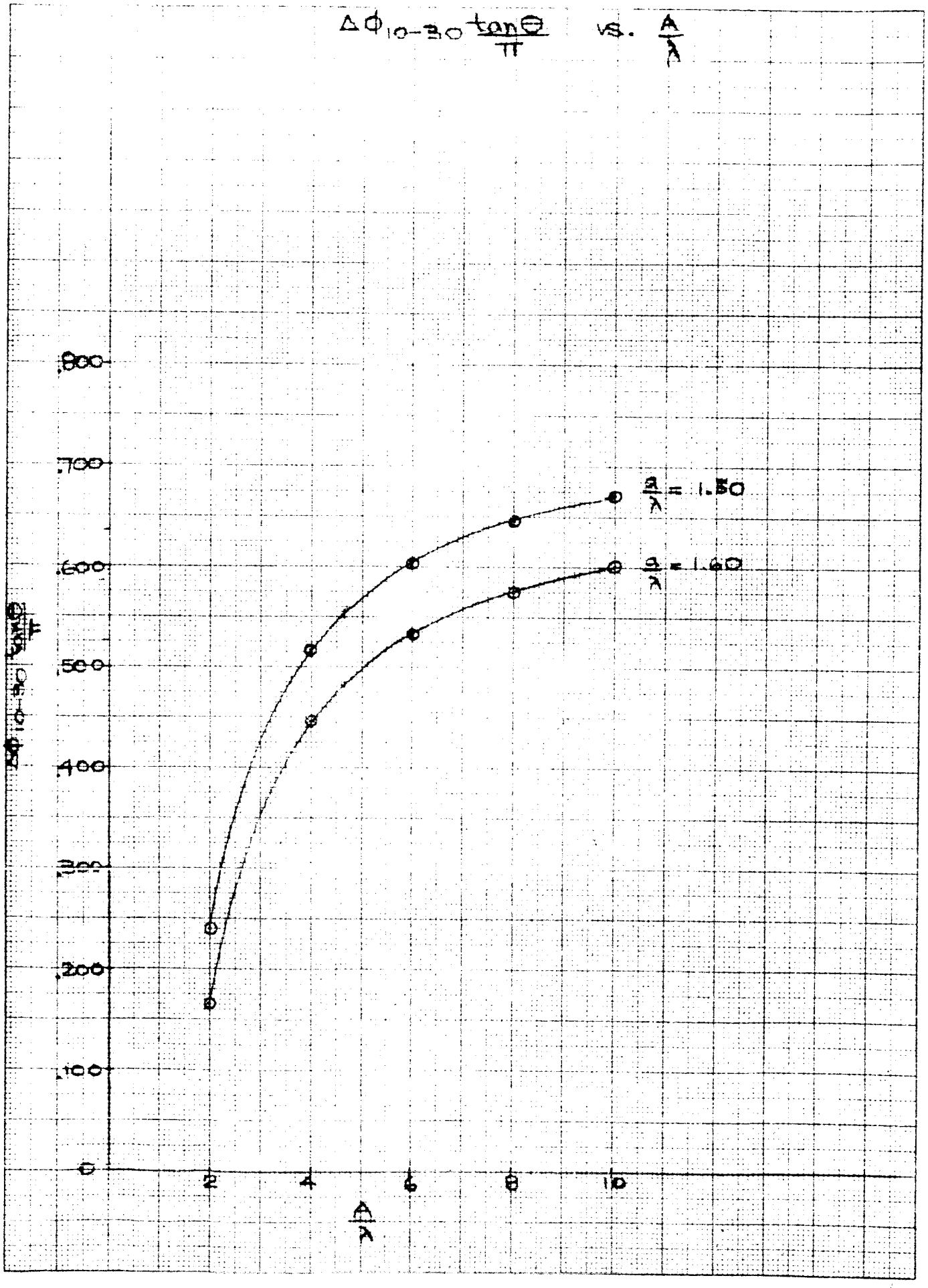

K+E 10 X 10 TO THE CM. 359-14
KEUFFEL & ESSER CO.

Graph #2

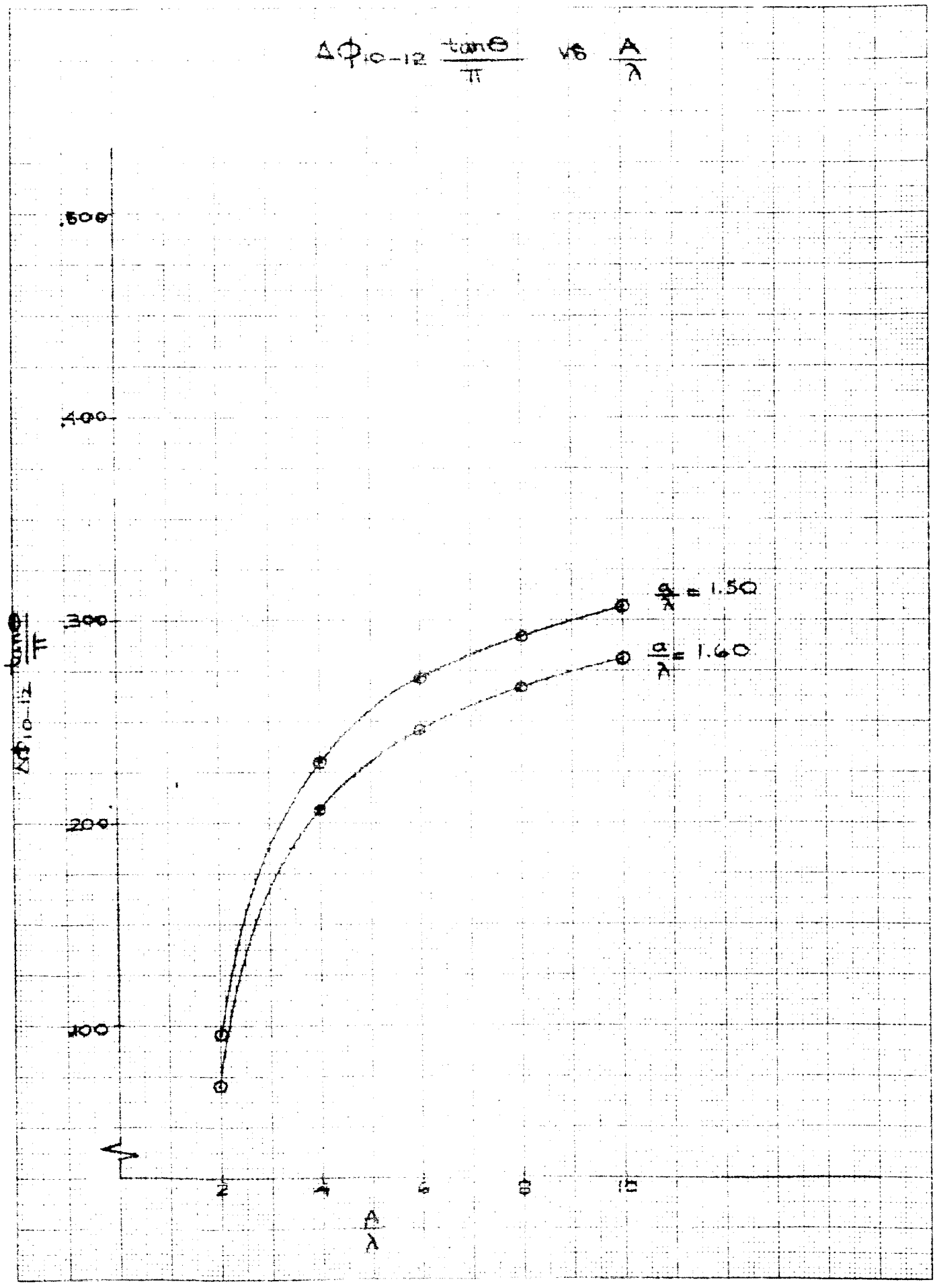

K+E 10 X 10 TO THE CM. 359-14 KEUFFEL & ESSER CO.

Graph #3

$\frac{\lambda}{2\pi} \Delta\theta_{10-30}$ vs. $\frac{a}{\lambda}$

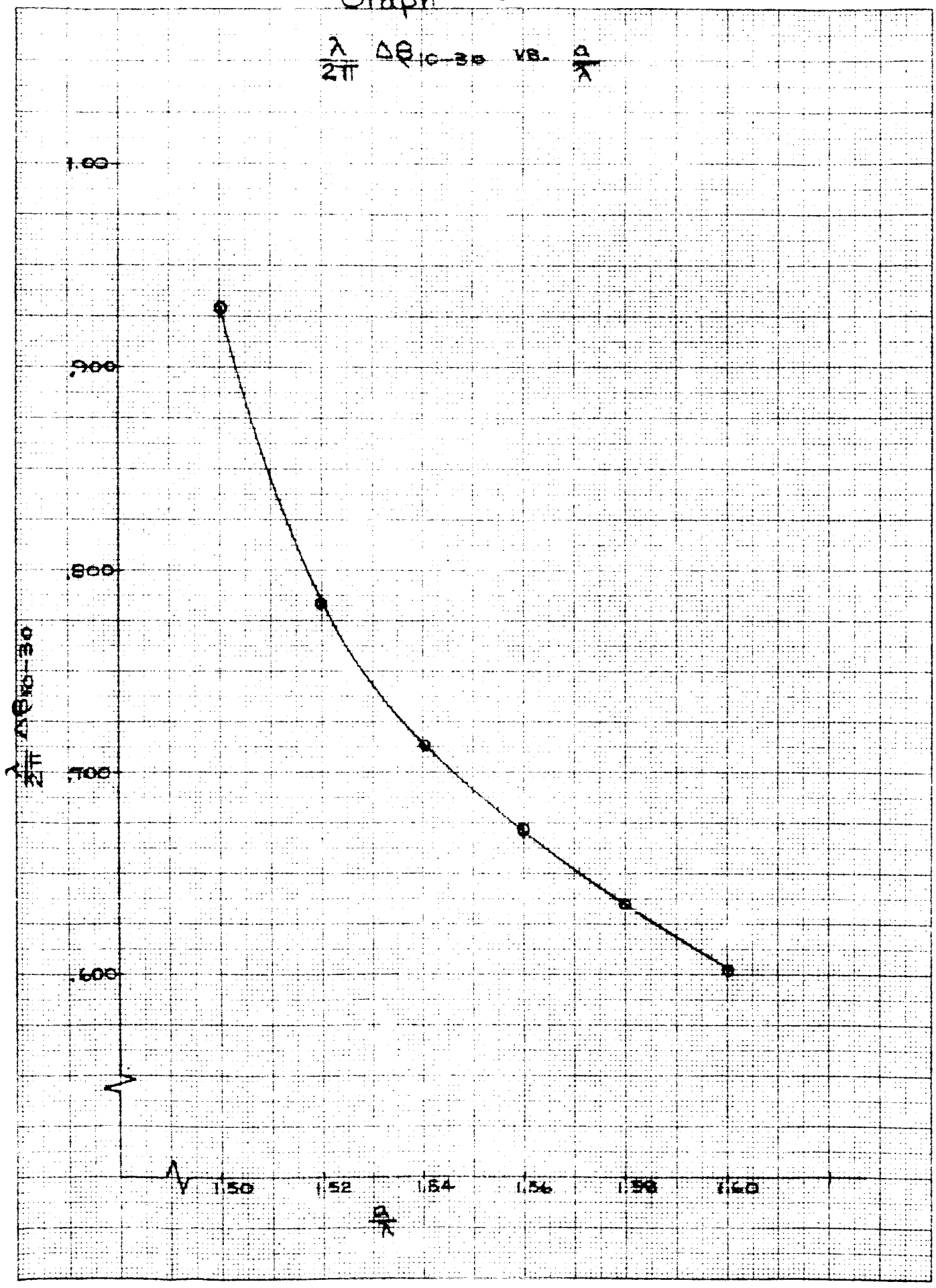

K+E 10 X 10 TO THE CM. 359-14
KEUFFEL & ESSER CO.

Graph #4

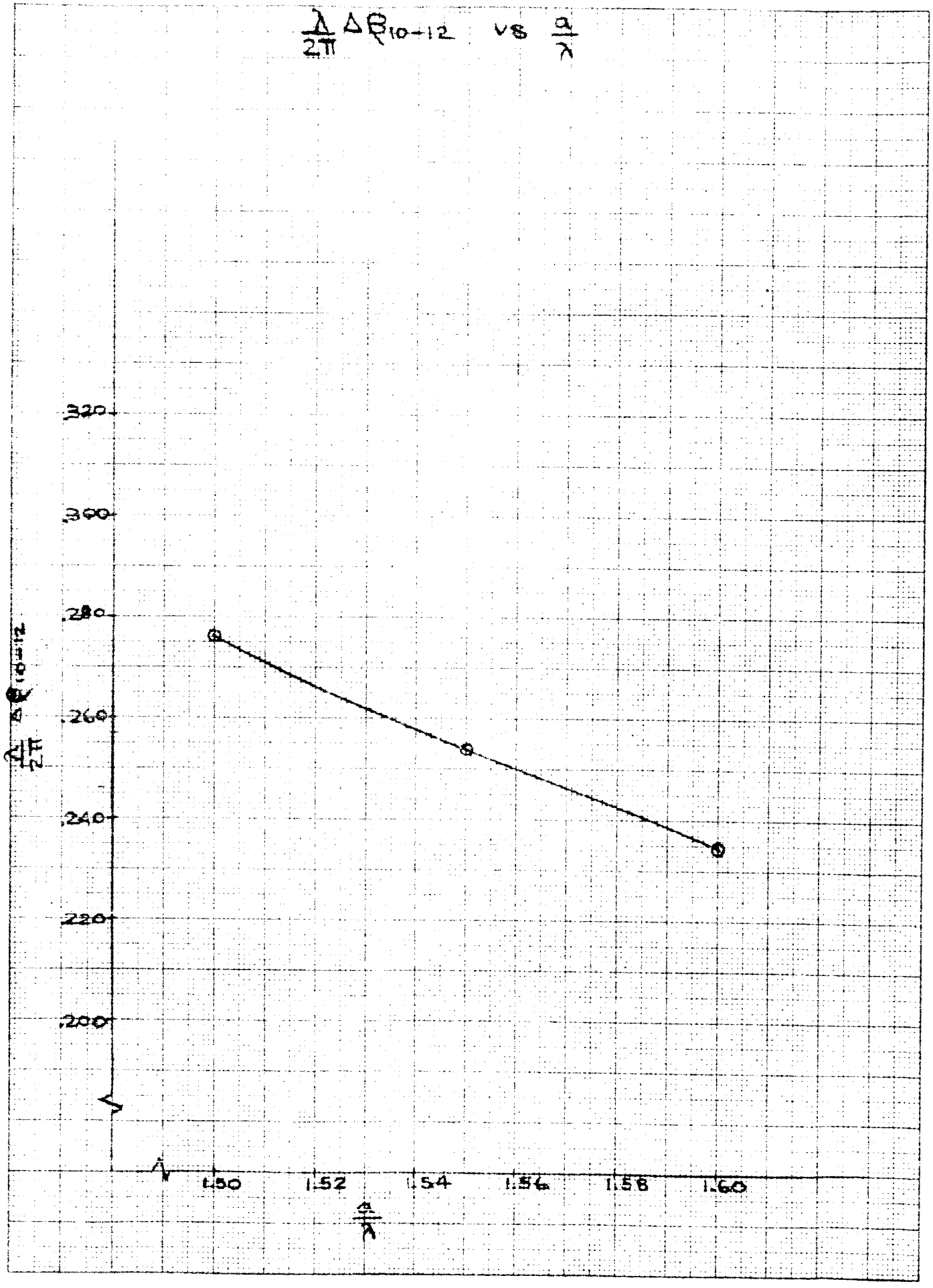

K+E 10 X 10 TO THE CM. 359-14 KEUFFEL & ESSER CO.

Graph #5

Regions of acceptable

$\Delta\Phi_{10-30}$ & $\Delta\Phi_{10-12}$

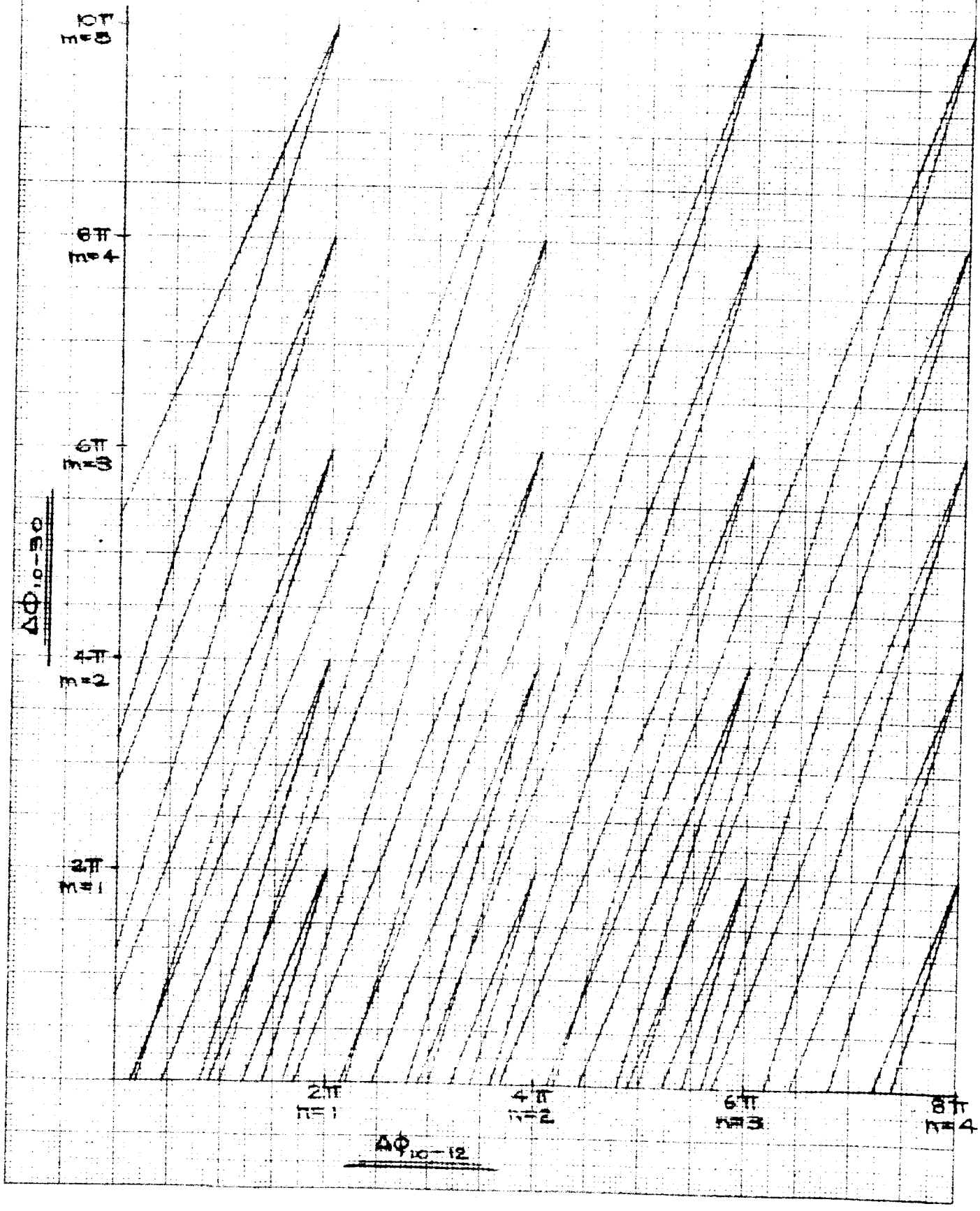

K+E 10 X 10 TO THE CM. 359-14

Graph #6

$\Delta\Phi_{11-20} \frac{\tan\theta}{\pi}$ vs. $\frac{A}{\lambda}$

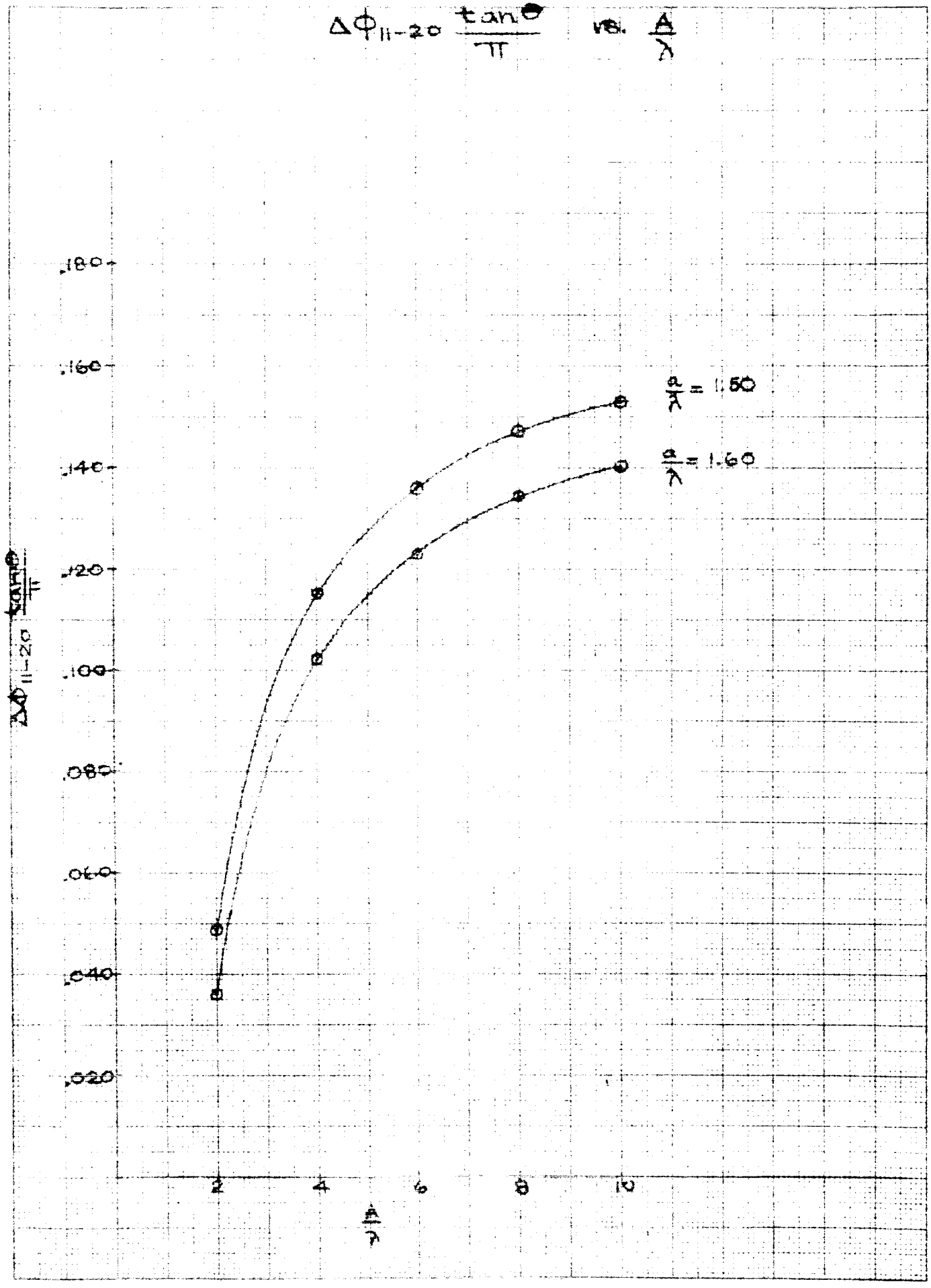

Graph #7

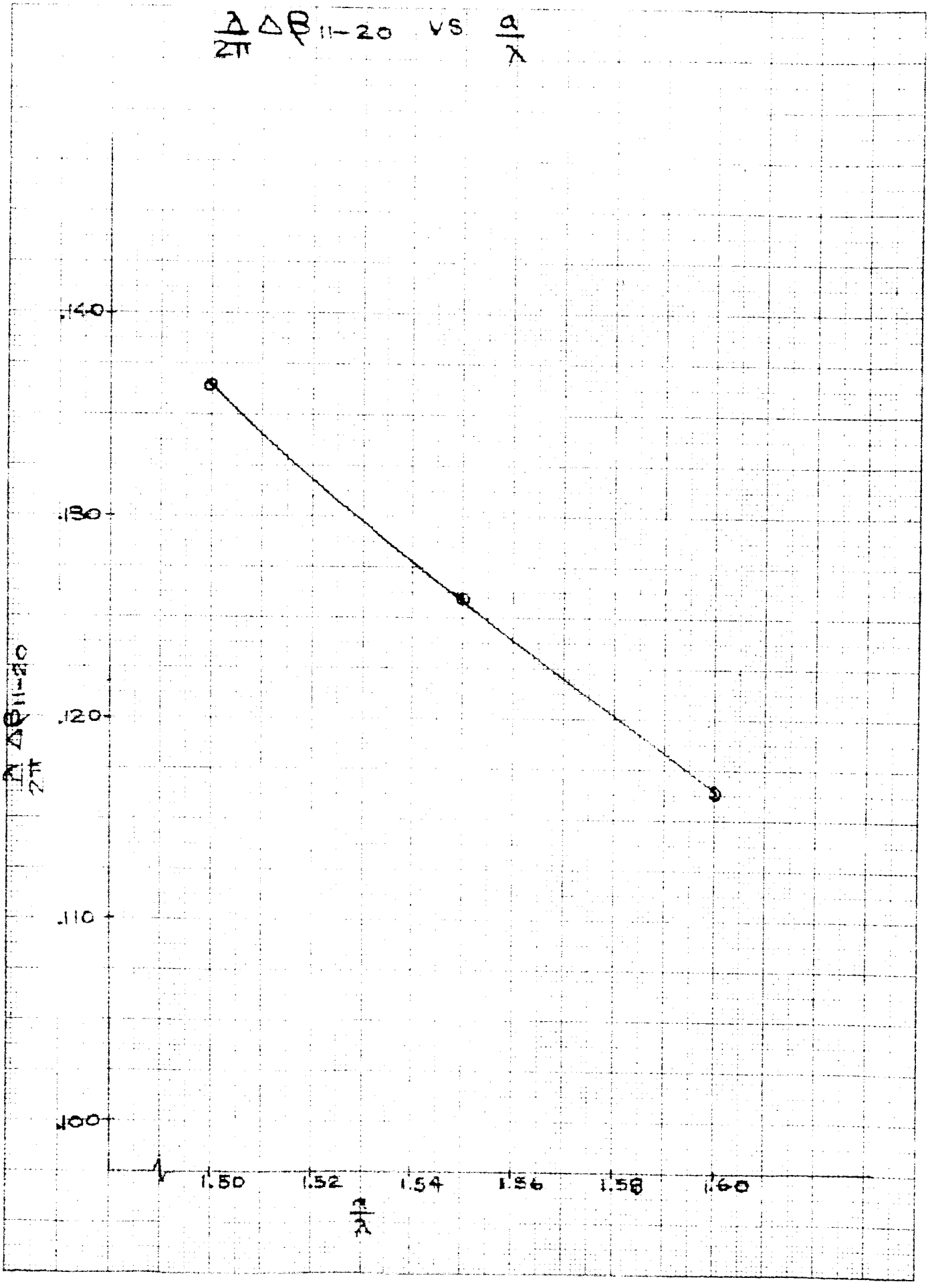
$\frac{\lambda}{2\pi}\Delta\beta_{11-20}$ vs $\frac{a}{\lambda}$
.140
.130
.120
.110
.100
$\frac{\lambda}{2\pi}\Delta\beta_{11-20}$
1.50
1.52
1.54
1.56
1.58
1.60
$\frac{a}{\lambda}$

Graph # 8

$\frac{\lambda}{2\pi} \Delta\theta_{11-20}$ vs $\frac{a}{\lambda}$

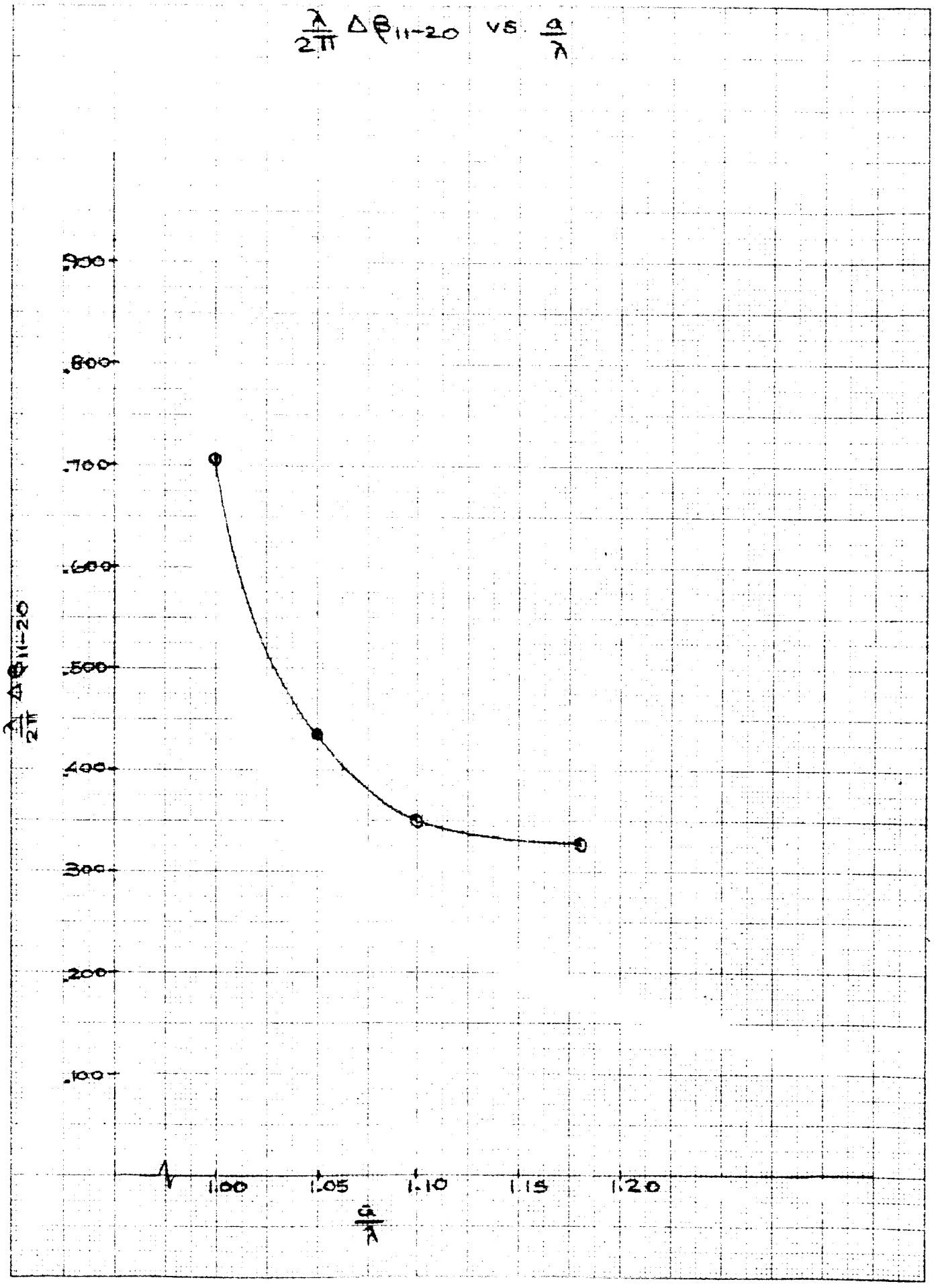

Graph #9

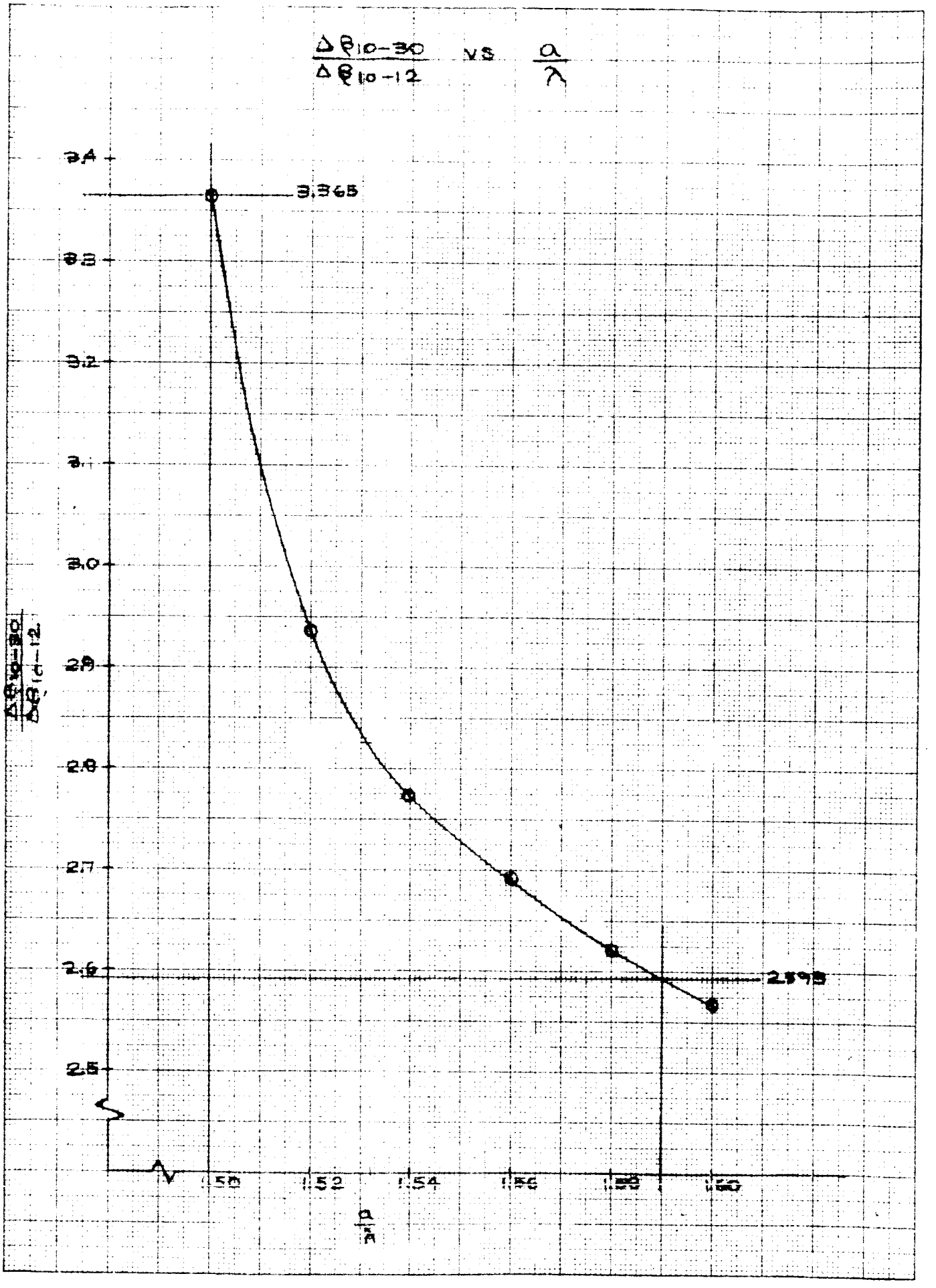
$\frac{\Delta\beta_{10-30}}{\Delta\beta_{10-12}}$ vs $\frac{a}{\lambda}$
3.4
3.3
3.2
3.1
3.0
2.9
2.8
2.7
2.6
2.5
3.365
2.595
1.50
1.52
1.54
1.56
1.58
1.60
$\frac{a}{\lambda}$
$\frac{\Delta\beta_{10-30}}{\Delta\beta_{10-12}}$

Experimental Results

The various characteristics of the multimode horn were measured and results have been previously reported during succeeding stages of the design. A summary of the performance of this feed (see Figure 9) is outlined below.

Table I shows the isolation of the developmental feed unit. The VSWR of this feed over the frequency bands of 2113 ±5 Mc and 2295 ±5 Mc is tabulated in Table II. Comprehensive amplitude and phase patterns have appeared in previous reports, and extensive patterns will be provided on the production feed units under JPL Contract 950678. For this reason only representative patterns are included in the Appendix. Results of phase center measurements indicate the best center of phase for the horn is 4" behind the aperture and phase patterns included in the Appendix are taken at this point.

Boresight roll error characteristics of the feed are tabulated in Table III. The null plane orthogonality measured appears in Table IV. Axial Ratio of the Sum and Difference Channel appear in Table V.

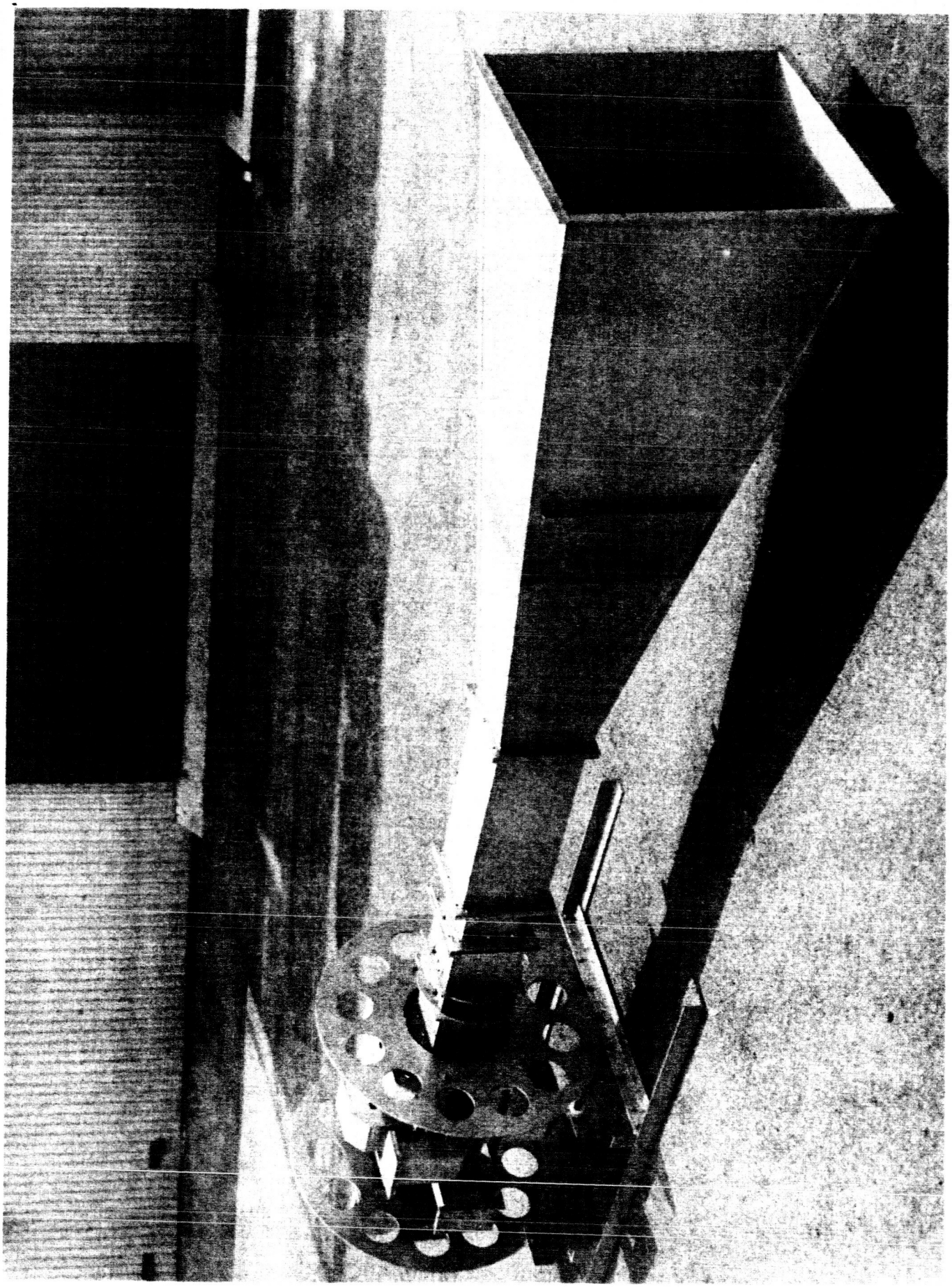

Figure 3 Low Noise Fend - Experimental Model

Table I

DSIF-SCM Low Noise Feed

Developmental Model

f = 2295 Mc								
	NΣ	NVΔ	NHΔ	NXΔ	OΣ	OVΔ	OHΔ	OXΔ
NΣ	X	40+	29	33.5	35.5	40+	40+	40+
NVΔ	40+	X	16.5	30	38.5	16	16.7	38
OVΔ	29	16.5	X	40+	40+	16.5	15	40+
OΣ	35.5	38.5	40+	40+	X	28.2	39.5	40
OVΔ	-	-	-	37.5	28.2	X	16.8	36.5
OHΔ	-	-	15	29.5	39	16.8	X	28
f = 2113								
NΣ	X	40+	40	34.3	37.8	40+	36.3	40+
OΣ	37.8	40+	40+	40+	X	40+	40+	32.2

Table II

SCM Feed VSWR vs Frequency

Freq. (mc)	NΣ	NVΔ	NHΔ	OΣ	OVΔ	OHΔ
2108	1.04			1.04		
2112	1.05			1.03		
2113	1.05			1.02		
2114	1.05			1.02		
2118	1.05			1.05		
2290	1.05	1.90	1.85	1.05	2.0	1.90
2293		1.30	1.31	1.04	1.36	1.30
2294	1.04	1.14	1.14	1.04	1.13	1.15
2295	1.05	1.02	1.04	1.03	1.02	1.03
2296	1.05	1.13	1.11	1.03	1.10	1.12
2297		1.32	1.29	1.03	1.34	1.33
2300	1.05	1.85	1.80	1.04	2.0	2.0

Table III

Boresight Movement vs Incident Linear Polarization

	Hour Angle	Declination
RCP Channel	0.12°	0.15°
LCP Channel	0.02°	0.08°

Table IV

DSIF-SCM Low Noise Feed
Null Plane Orthogonality

	Angle Between Null Plane
RCP Error Channels	89°
LCP Error Channel	89°

Table V

DSIF-SCM Low Noise Feed
Axial Ratio

f = 2295 Mc	Axial Ratio
NΣ	0.1 db
NVΔ	0.9
NHΔ	1.4
OΣ	0.3
OVΔ	1.1
OHΔ	1.4
f = 2113 Mc	
NΣ	1.2
OΣ	1.3

Additional Study

Several modifications of the basic multimode feed were investigated during the course of this program. One of the main limitations on the basic design is that it provides sidelobe calcellation at only one frequency. Two techniques to provide dual frequency pattern control were investigated. These are:

1. Separation of modes
2. Elimination of the constriction in the multimode matching section.

Several possible methods of separating the modes are possible, but most techniques require a precise knowledge of the mode excitation coefficients and an accurate prediction of relative phasing. Since these problems were not satisfactorily solved, this technique is impractical at the present. A further discussion of this topic appears in the monthly progress reports.

The second technique, elimination of the matching constriction, appears to have some practical application. An X-band experimental model was fabricated which provided dual frequency mode control and phased all the modes in one section, thus eliminating the constriction. Results of this experiment, reported in the November progress report, were only partially conclusive. The technique does appear to work; however, the X-band circular polarizer used was not good enough to provide satisfactory results. A further program to investigate this technique applied to the S-band SCM feed would be worth while.

As was mentioned, some theoretical calculation of the mode excitation coefficients and prediction of radiation patterns was also attempted. While correlation of theoretical with experimental results was not completely accomplished, a basis was made for future experimental work in determination of the actual excitation coefficients and phase control.

The problem of matching the modes into the multimode horn was briefly treated in the November report also. It may be possible to improve the overall matching problem by a different choice of geometry at the junction of the four guides and the multimode guide. This, however, requires an experimental program to investigate the various possible configurations.

APPENDIX A

SCM SUPPRESSED SIDELOBE FEED

DEVELOPMENTAL UNIT

Abbreviations on Patterns

FS	=	full scale
NS	=	normal sum
OS	=	orthogonal sum
OHD	=	orthogonal horizontal difference, etc.
CR	=	center of rotation behind aperture (inches)
HCO or HC	=	horizontal cut orientation
VCO or VC	=	vertical cut orientation
RC	=	right circular polarization, etc.

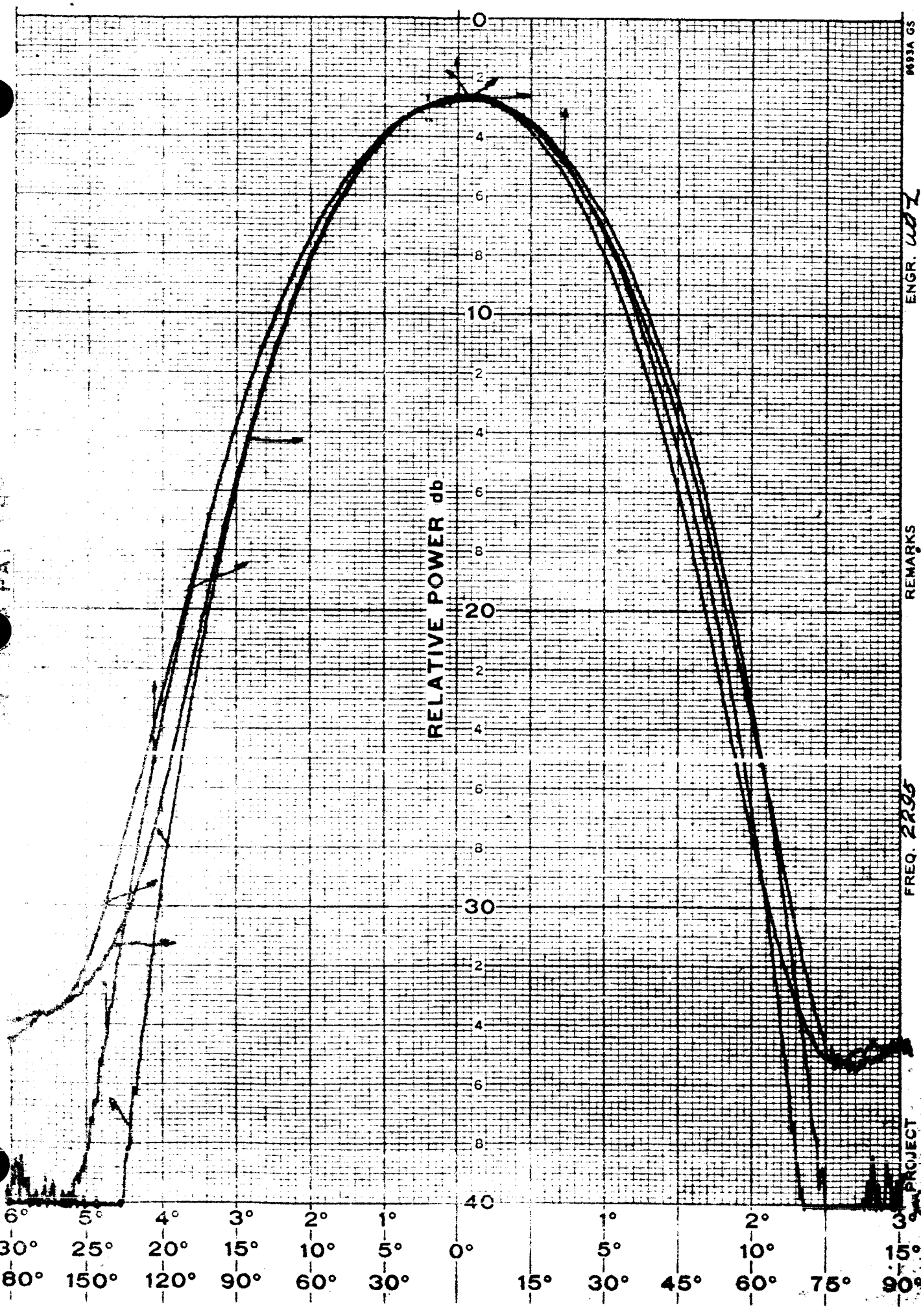

RELATIVE POWER db
0
2
4
6
8
10
20
30
40
6° 5° 4° 3° 2° 1° 1° 2° 3°
30° 25° 20° 15° 10° 5° 0° 5° 10° 15°
180° 150° 120° 90° 60° 30° 15° 30° 45° 60° 75° 90°
PROJECT
FREQ. 2295
REMARKS
ENGR.
DATE 11-26-63
PLANE NI - NC - CR-4

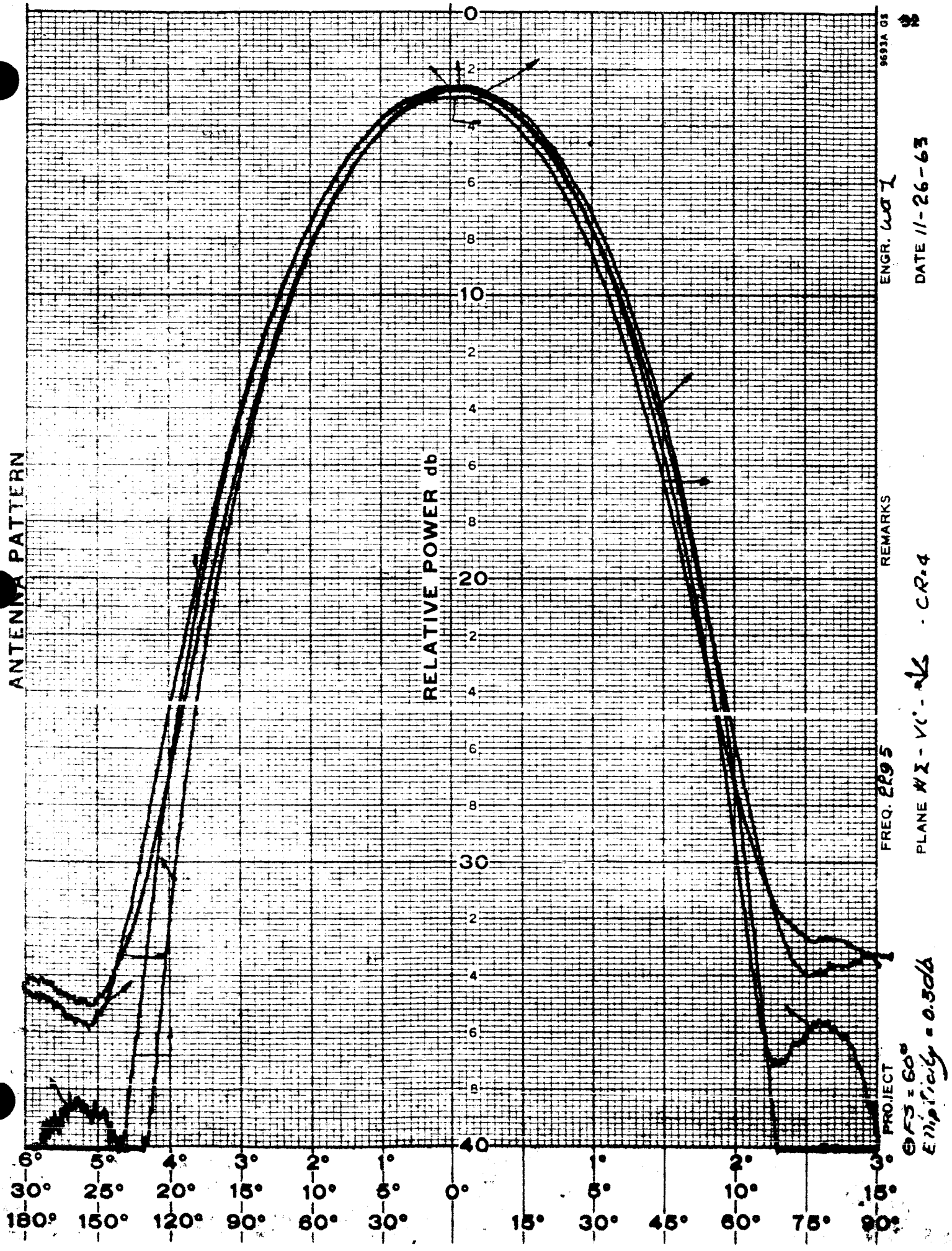
ANTENNA PATTERN
RELATIVE POWER db
0
2
4
6
8
10
2
4
6
8
20
2
4
6
8
30
2
4
6
8
40
6° 5° 4° 3° 2° 1° 1° 2° 3°
30° 25° 20° 15° 10° 5° 0° 5° 10° 15°
180° 150° 120° 90° 60° 30° 15° 30° 45° 60° 75° 90°
PROJECT
FREQ. 2295
REMARKS
ENGR.
DATE 11-26-63
PLANE
CR-4
9693A 03

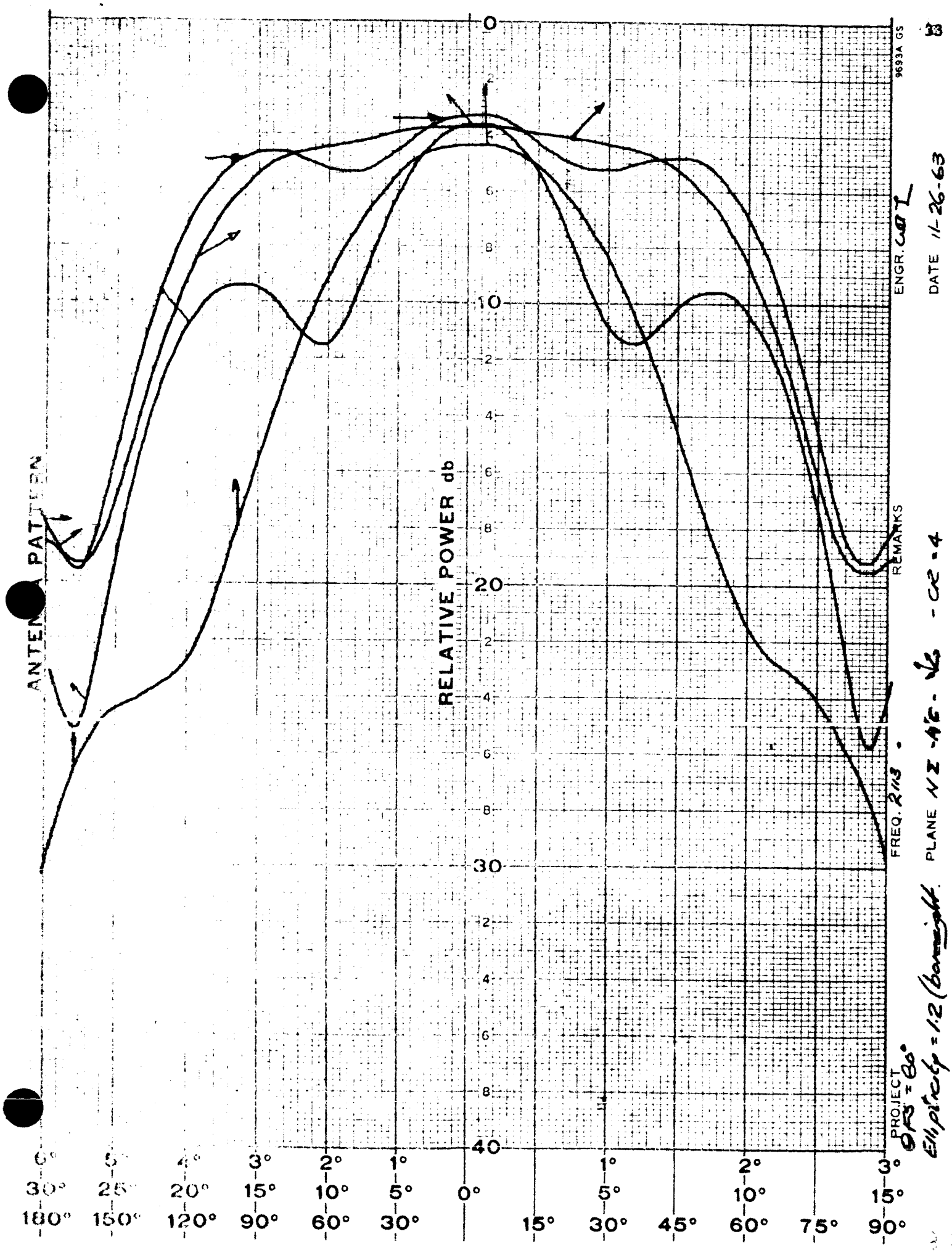

ANTENNA PATTERN
RELATIVE POWER db
0
2
4
6
8
10
2
4
6
8
20
2
4
6
8
30
2
4
6
8
40
6° 5° 4° 3° 2° 1° 1° 2° 3°
30° 25° 20° 15° 10° 5° 0° 5° 10° 15°
180° 150° 120° 90° 60° 30° 15° 30° 45° 60° 75° 90°
9693A GS
ENGR. [illegible]
DATE 11-26-63
REMARKS
FREQ. 2113
PLANE NΣ - AE - [illegible] - CR = 4
PROJECT
DFS = 80°
Ellipticity = 1.2 (boresight)

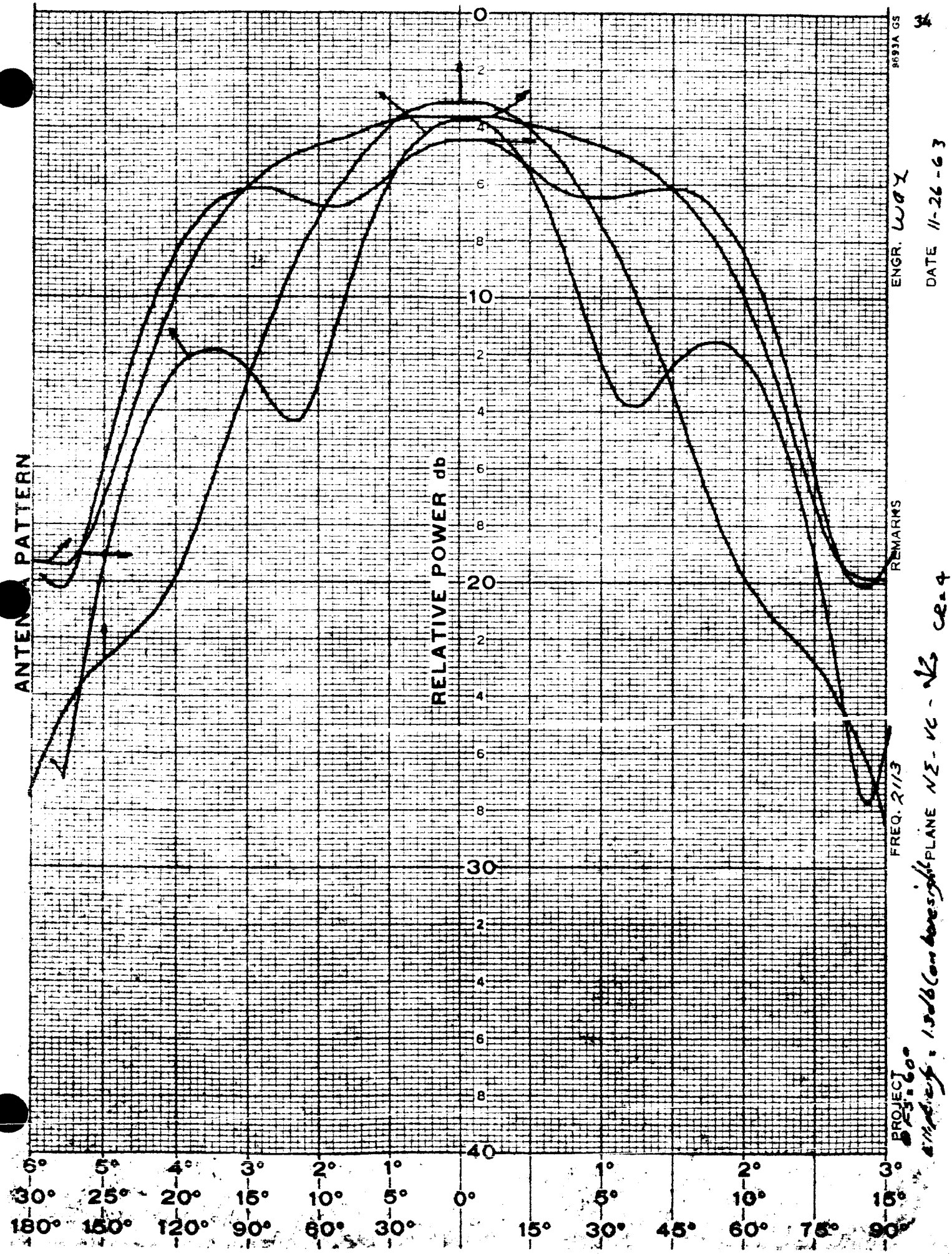
ANTENNA PATTERN
RELATIVE POWER db
0
2
4
6
8
10
20
30
40
6° 5° 4° 3° 2° 1° 1° 2° 3°
30° 25° 20° 15° 10° 5° 0° 5° 10° 15°
180° 150° 120° 90° 60° 30° 15° 30° 45° 60° 75° 90°
8693A GS
ENGR. WAL
DATE 11-26-63
REMARKS
FREQ. 2113
PLANE NE - VC - VS
PROJECT
CR-4

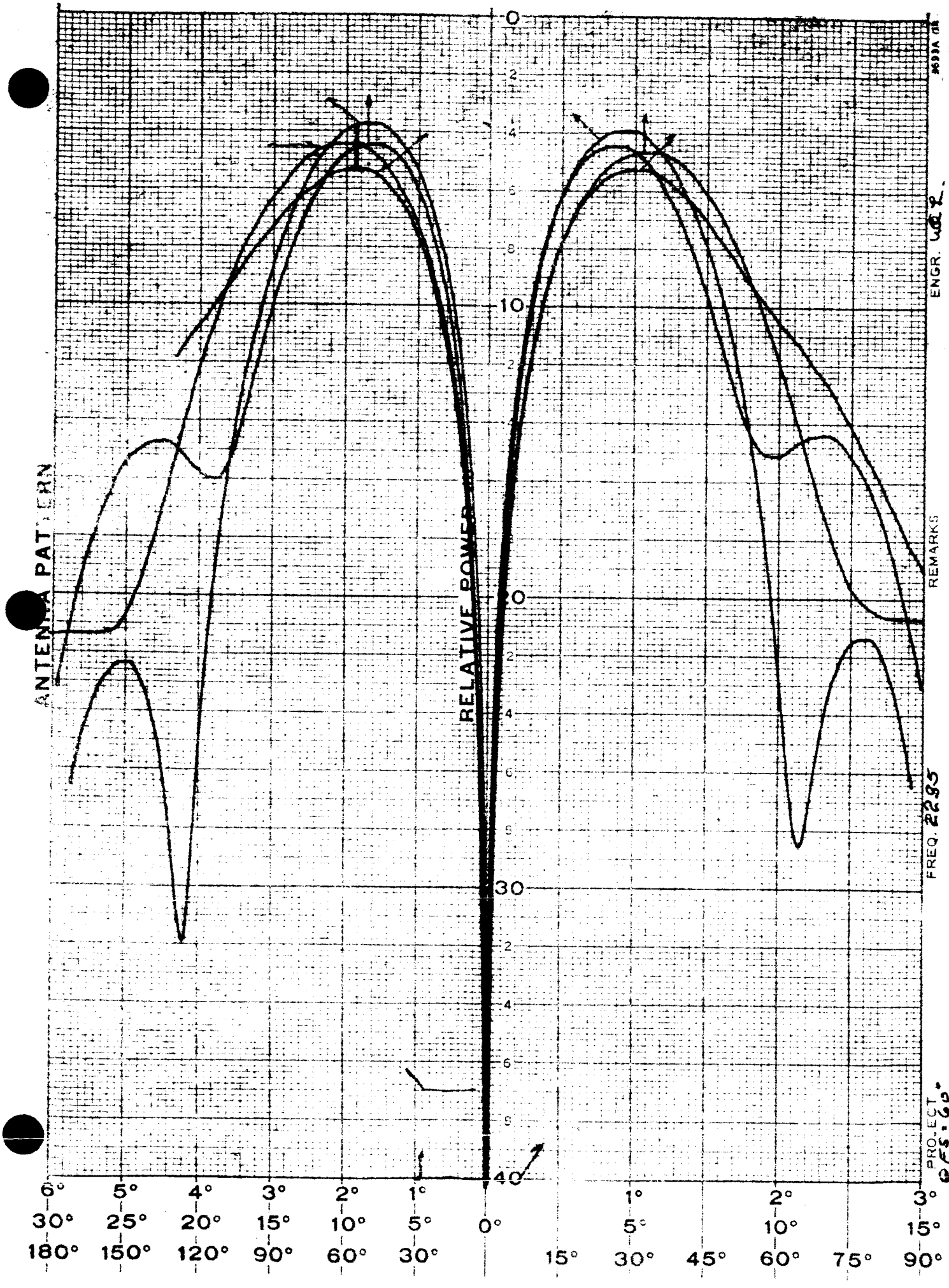
ANTENNA PATTERN
RELATIVE POWER
0
2
4
6
8
10
20
30
40
6° 5° 4° 3° 2° 1° 0° 1° 2° 3°
30° 25° 20° 15° 10° 5° 15° 5° 10° 15°
180° 150° 120° 90° 60° 30° 15° 30° 45° 60° 75° 90°
PROJECT
QFS=60°
Ellipticity = 1.4db.
FREQ. 2295
PLANE NHA - HC - Vs - Cl=4
REMARKS
ENGR.
DATE 11-26-63

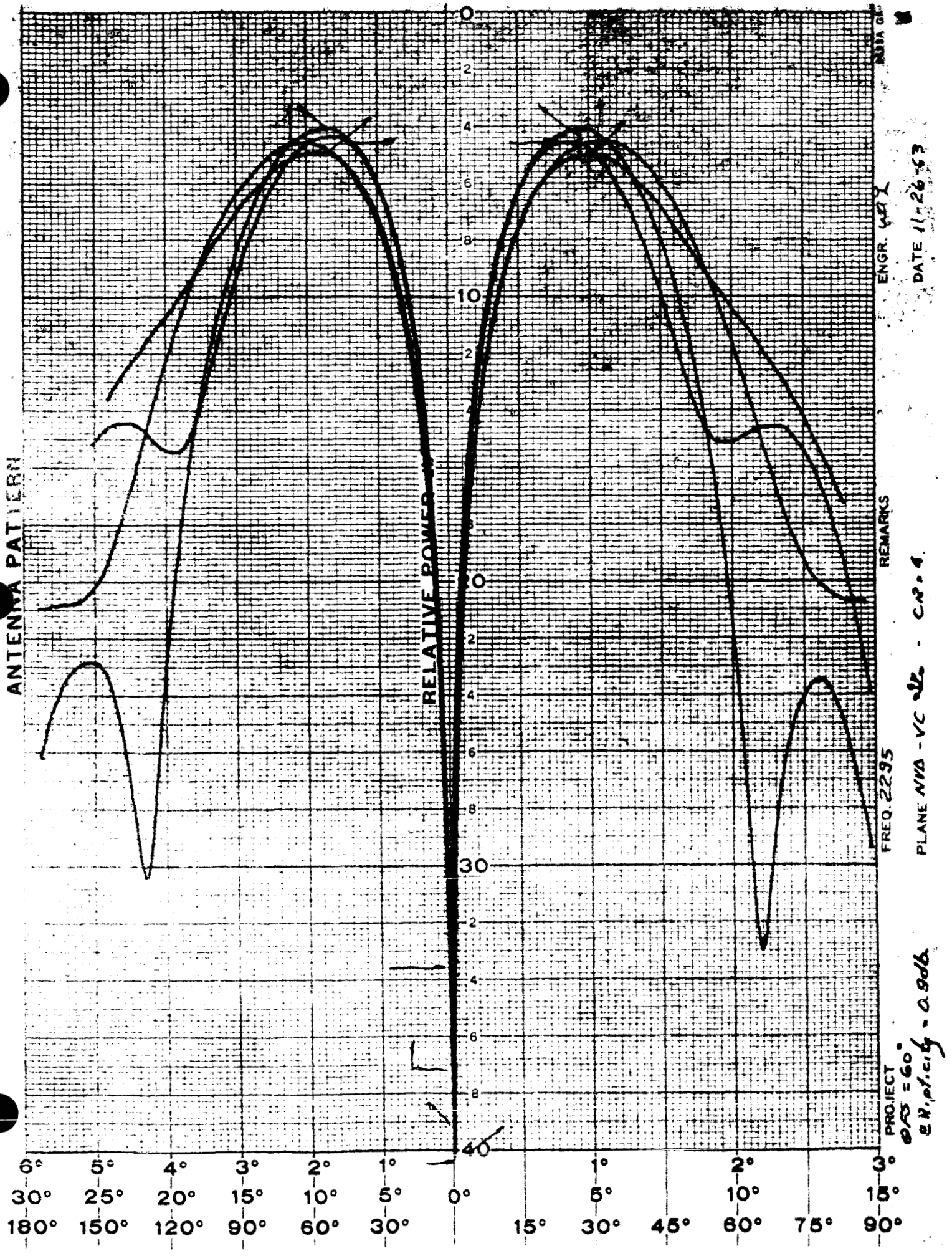
ANTENNA PATTERN
RELATIVE POWER
0
2
4
6
8
10
20
30
40
6° 5° 4° 3° 2° 1° 1° 2° 3°
30° 25° 20° 15° 10° 5° 0° 5° 10° 15°
180° 150° 120° 90° 60° 30° 15° 30° 45° 60° 75° 90°
PROJECT
ENGR.
DATE 11-26-63
REMARKS
FREQ. 2295
PLANE NVD - VC - CR-4
PROJECT
OFS = 60°
Rip.city - 0.9db

APPENDIX B

CIRCULAR POLARIZED PATTERNS

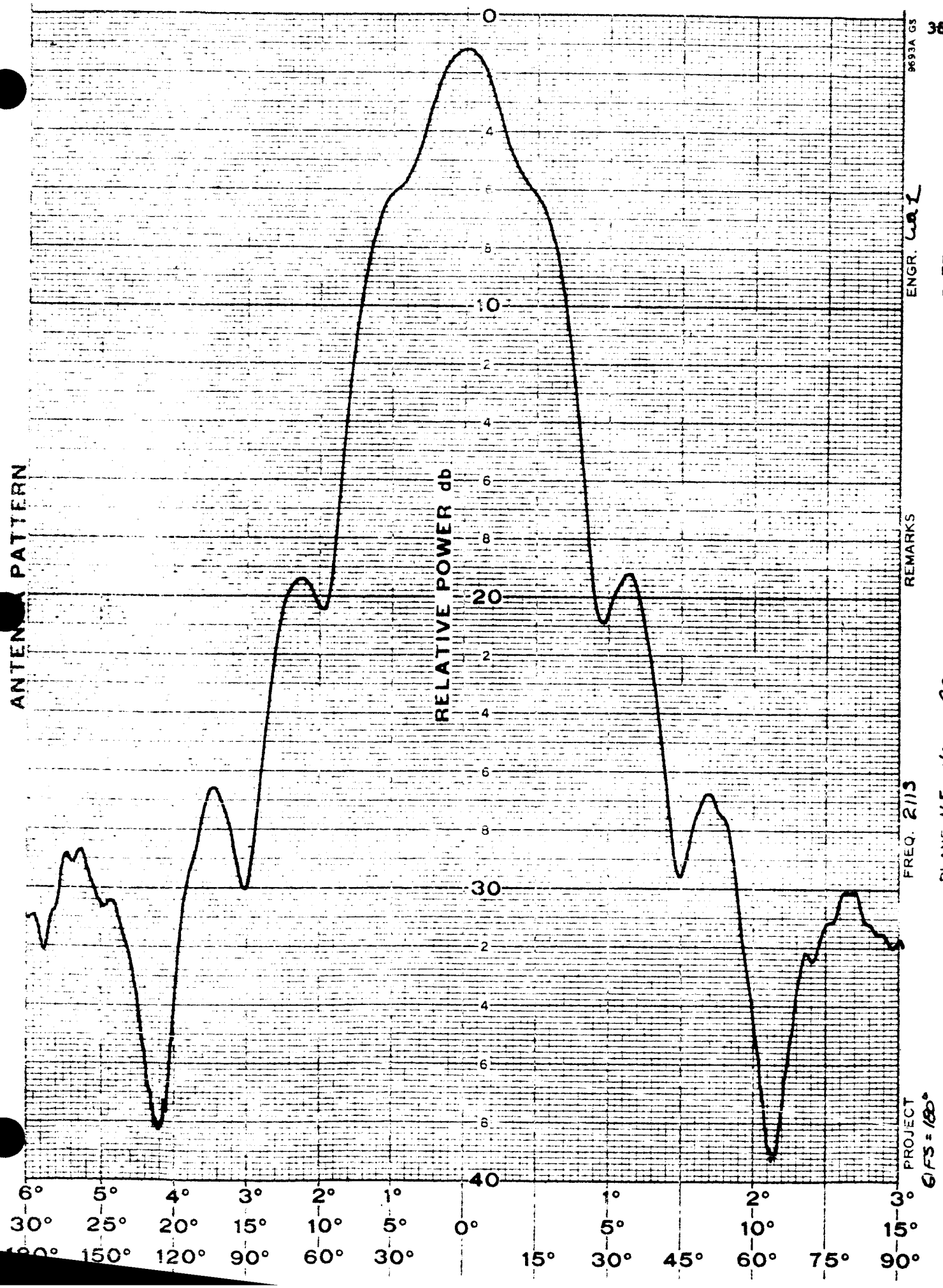
ANTENNA PATTERN
RELATIVE POWER db
0
4
6
8
10
2
4
6
8
20
2
4
6
8
30
2
4
6
8
40
6° 5° 4° 3° 2° 1° 1° 2° 3°
30° 25° 20° 15° 10° 5° 0° 5° 10° 15°
180° 150° 120° 90° 60° 30° 15° 30° 45° 60° 75° 90°
9693A GS
ENGR. WAL
DATE 11-14-63
REMARKS
FREQ. 2113
PLANE NΣ - HCO - RC
CR = 4
PROJECT
GFS = 180°

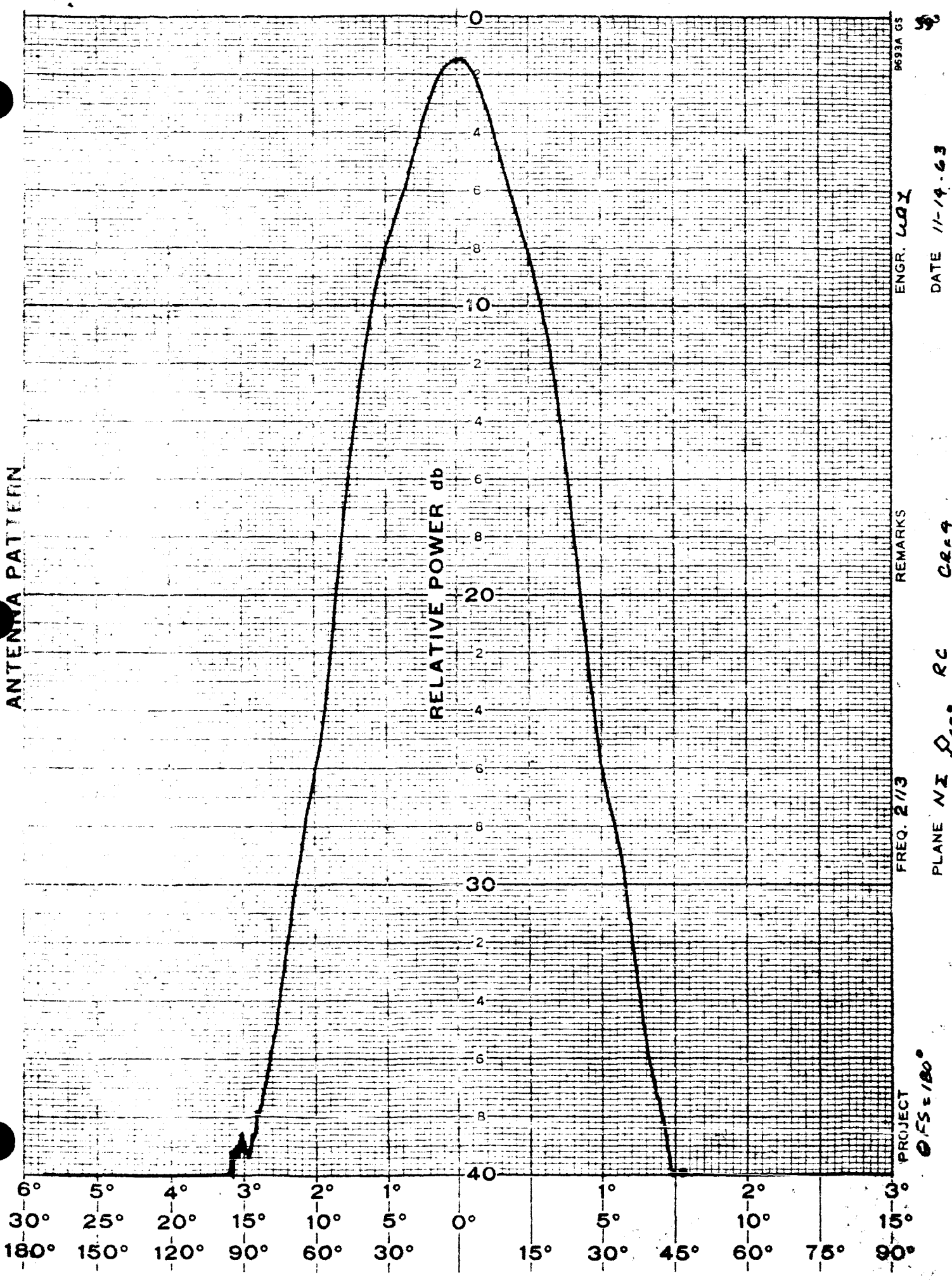
ANTENNA PATTERN
RELATIVE POWER db
0
2
4
6
8
10
2
4
6
8
20
2
4
6
8
30
2
4
6
8
40
6° 5° 4° 3° 2° 1° 1° 2° 3°
30° 25° 20° 15° 10° 5° 0° 5° 10° 15°
180° 150° 120° 90° 60° 30° 15° 30° 45° 60° 75° 90°
PROJECT
FREQ. 2113
REMARKS
ENGR.
DATE 11-14-63
PLANE NI
RC
CR=4
8693A GS

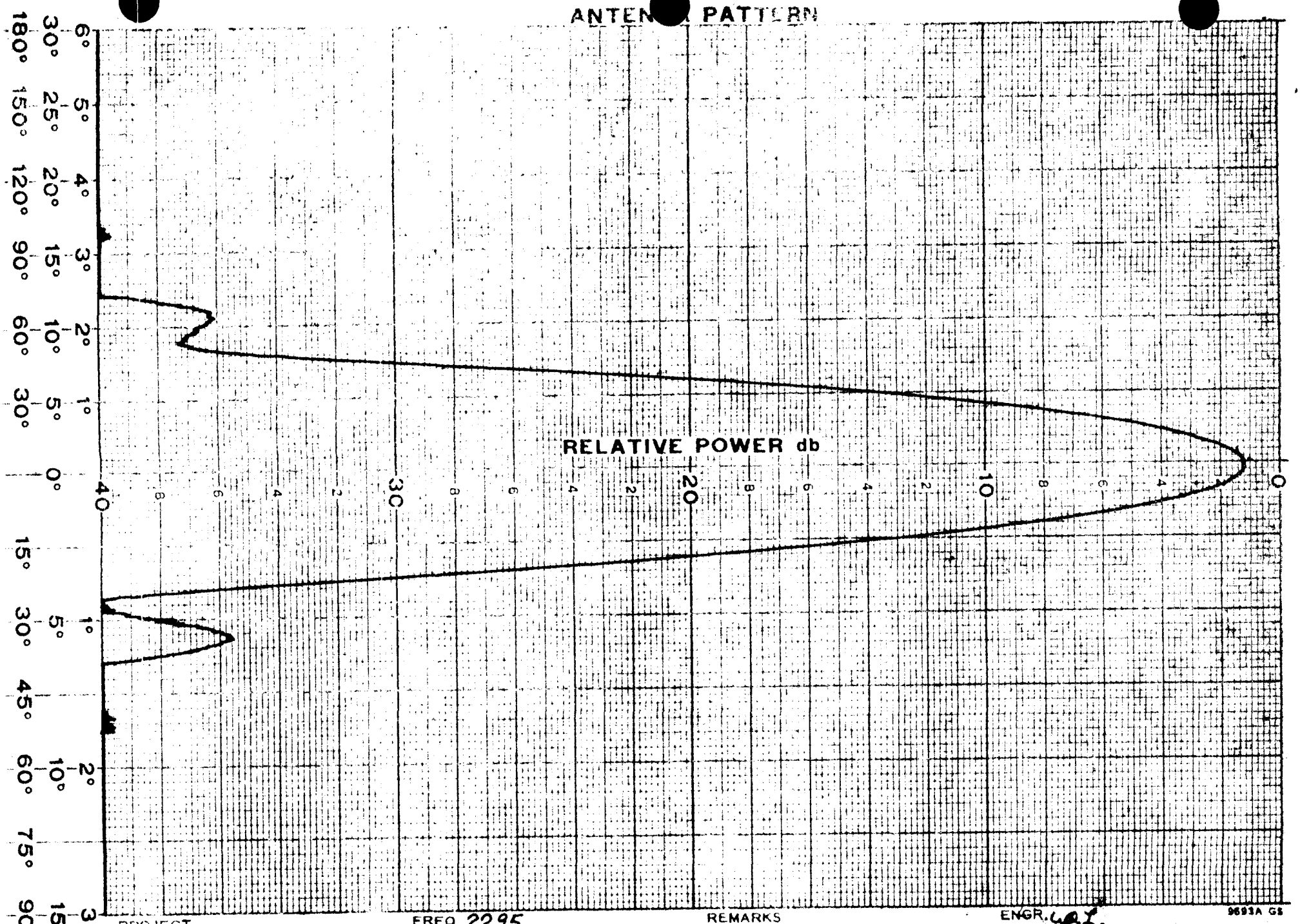

PROJECT

⊖ FS = 180°

FREQ. 2295

REMARKS

ENGR. W.L.

PLANE NΣ - HCO - RC

CR = 4

DATE 11-14-63

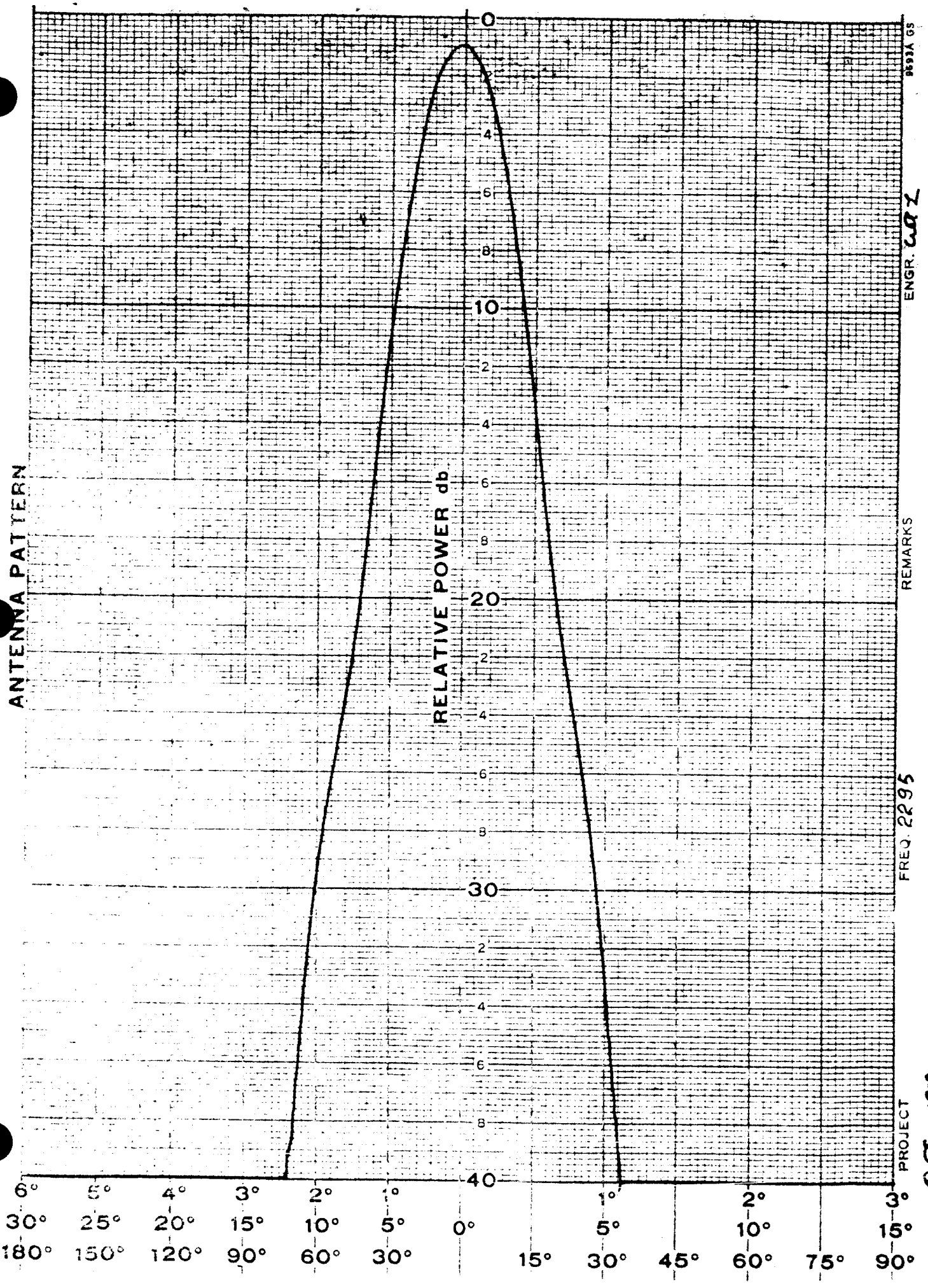
ANTENNA PATTERN
RELATIVE POWER db
0
4
6
8
10
2
4
6
8
20
2
4
6
8
30
2
4
6
8
40
6° 5° 4° 3° 2° 1° 1° 2° 3°
30° 25° 20° 15° 10° 5° 0° 5° 10° 15°
180° 150° 120° 90° 60° 30° 15° 30° 45° 60° 75° 90°
PROJECT
FREQ. 2295
REMARKS
ENGR.
DATE 11-14-63
PLANE NE RC CR=4.
45°
FS. =180°

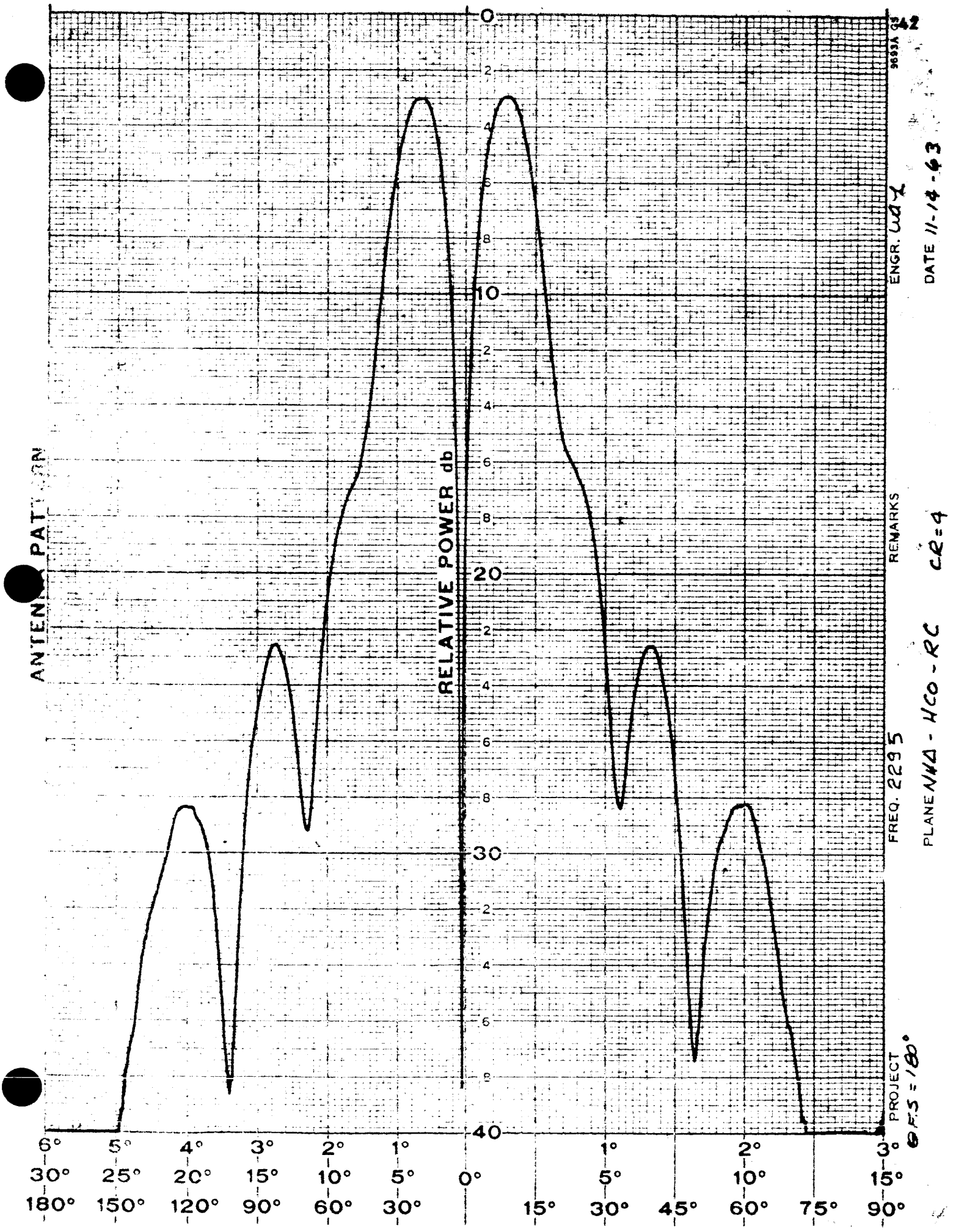

ANTENNA PATTERN
RELATIVE POWER db
0
2
4
6
8
10
20
30
40
6° 5° 4° 3° 2° 1° 1° 2° 3°
30° 25° 20° 15° 10° 5° 0° 5° 10° 15°
180° 150° 120° 90° 60° 30° 15° 30° 45° 60° 75° 90°
9693A
42
ENGR. WAL
DATE 11-14-63
REMARKS
CR=4
FREQ. 2295
PLANE NHA - HCO - RC
PROJECT
GFS = 180°

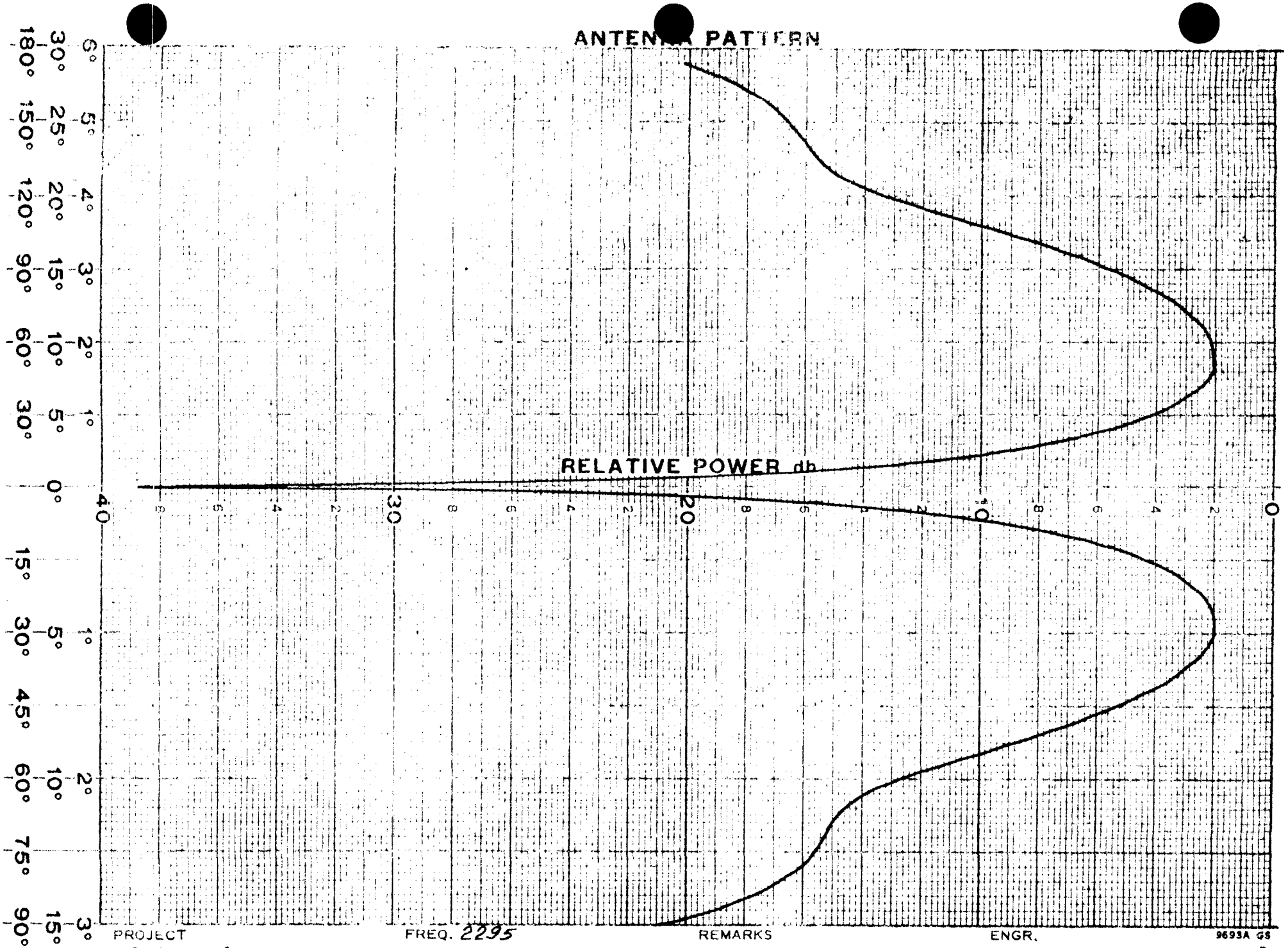

PROJECT

θ FS = 60°

FREQ. 2295

REMARKS

ENGR.

9693A GS

PLANE NHΔ - HCO - RC. CR = 4

DATE 11-14-63

43

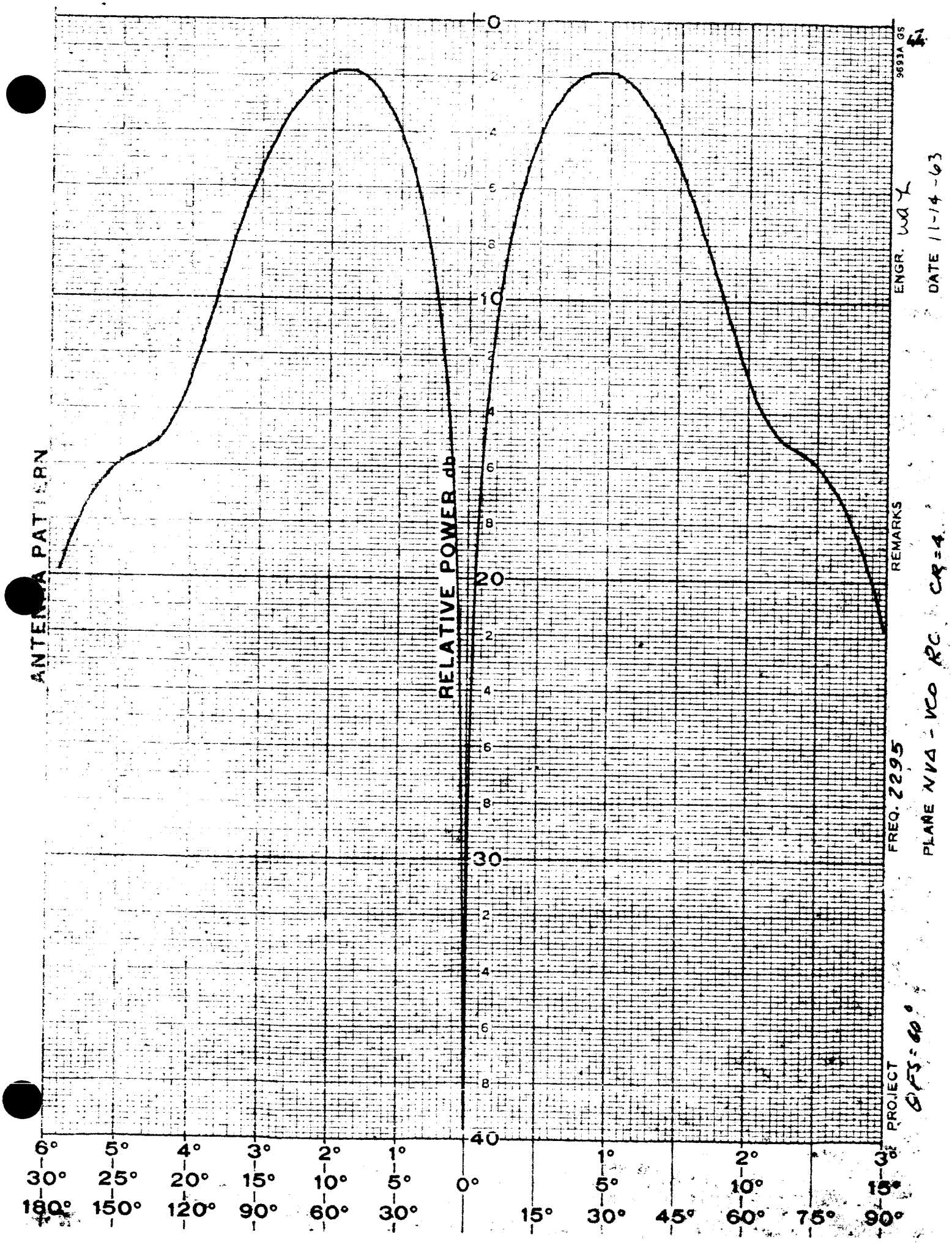
ANTENNA PATTERN
RELATIVE POWER db
0
2
4
6
8
10
20
30
40
6° 5° 4° 3° 2° 1° 1° 2° 3°
30° 25° 20° 15° 10° 5° 0° 5° 10° 15°
180° 150° 120° 90° 60° 30° 15° 30° 45° 60° 75° 90°
9693A GS
ENGR. WAL
DATE 11-14-63
REMARKS
FREQ. 2295
PLANE NVA - VCO RC CR=4
PROJECT
QFS: 60°

APPENDIX C

REPRESENTATIVE PHASE PATTERNS TAKEN ABOUT A CENTER OF ROTATION 4" BEHIND APERTURE

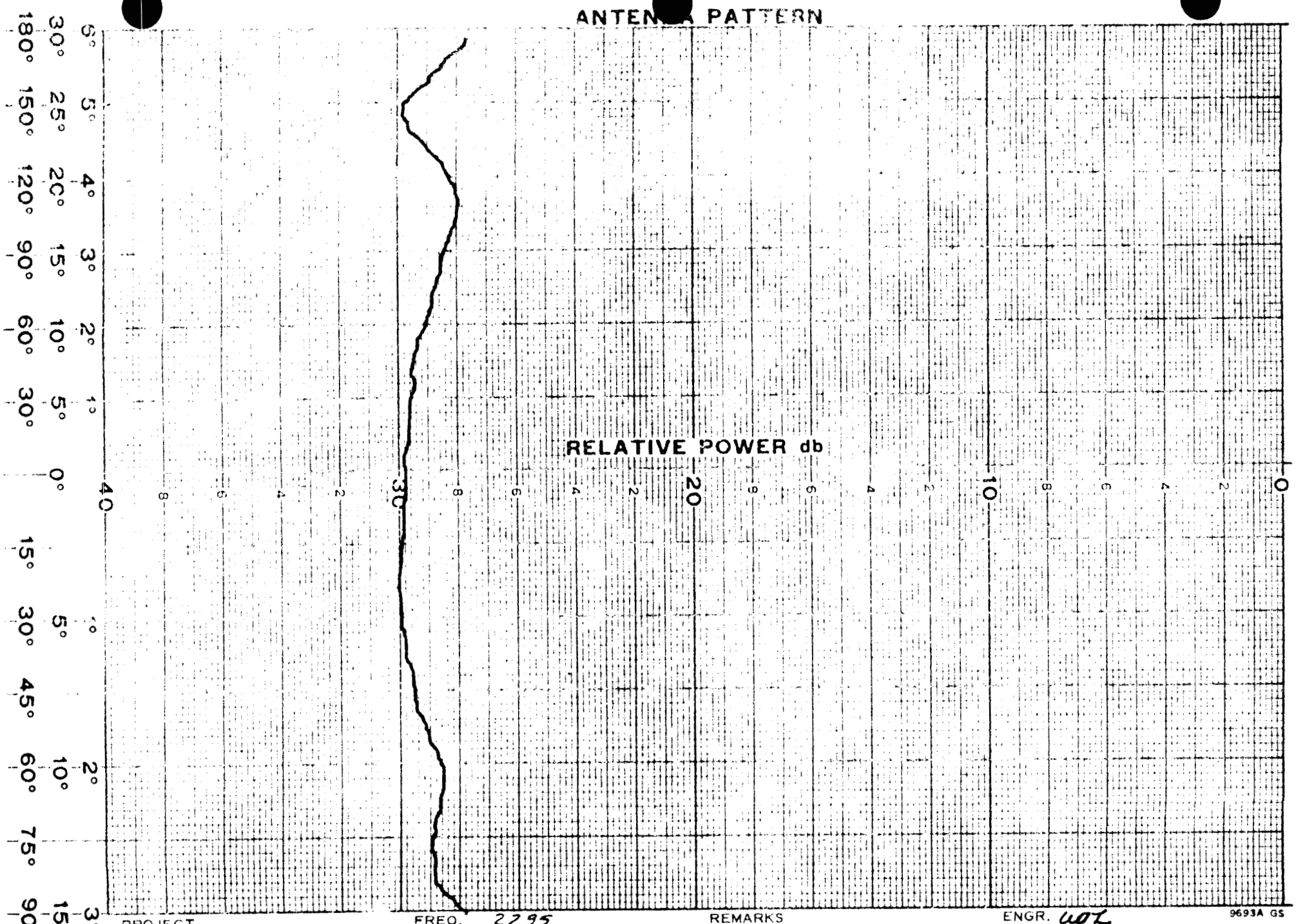
ANTENNA PATTERN
RELATIVE POWER db
0
10
20
30
40
180° 150° 120° 90° 60° 30° 0° 15° 30° 45° 60° 75° 90°
30° 25° 20° 15° 10° 5° 0° 5° 10° 2° 15° 3°
5° 5° 4° 3° 2° 1° 1° 2° 3°
PROJECT
θ-3 = 60°
φ = 180°/36db.
FREQ. 2295
REMARKS
ENGR. WDL
9693A GS
PLANE NΣ - HC - RC CR = 4
DATE 11-19-63

46

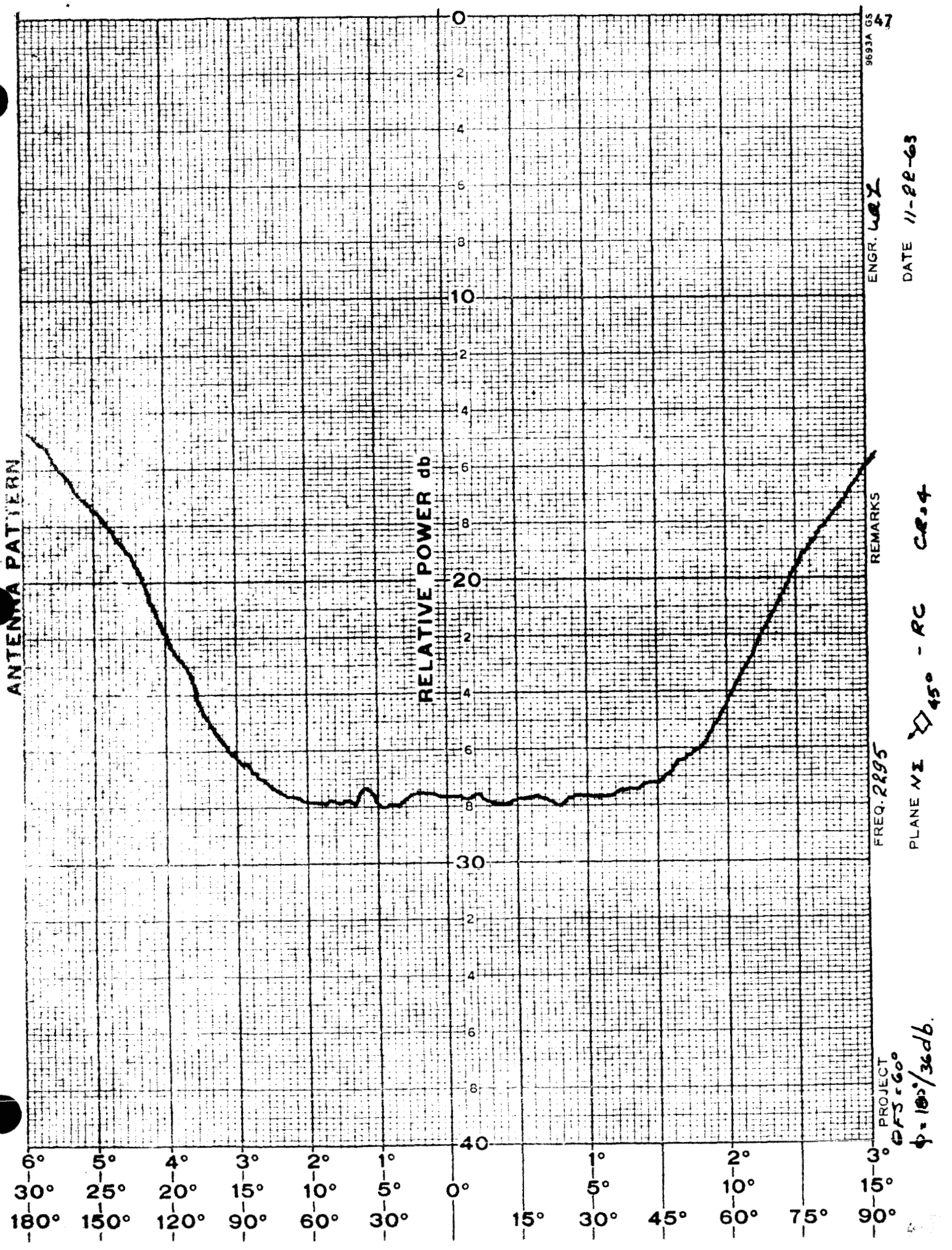
ANTENNA PATTERN
RELATIVE POWER db
0
2
4
6
8
10
20
30
40
6° 5° 4° 3° 2° 1° 1° 2° 3°
30° 25° 20° 15° 10° 5° 0° 5° 10° 15°
180° 150° 120° 90° 60° 30° 15° 30° 45° 60° 75° 90°
9693A GS 47
ENGR. WRL
DATE 11-22-63
REMARKS
FREQ. 2295
PLANE NI 45° - RC CR-4
PROJECT
DFS = 60°
φ = 180°/36db.

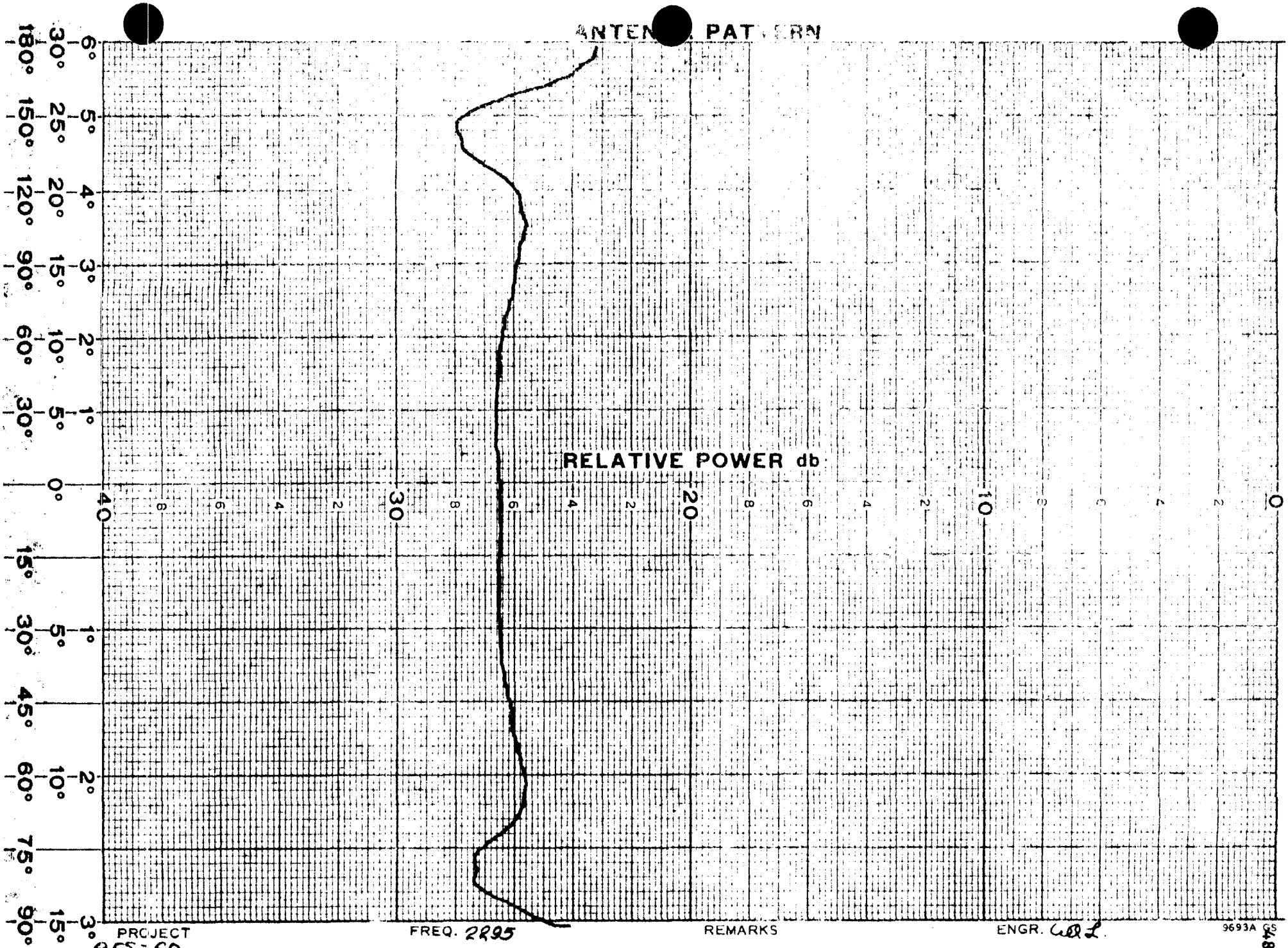

PROJECT
θFS = 60
φ - 180°/38db.

FREQ. 2295

PLANE NΣ - VC - RC

REMARKS

CR = 4.

ENGR. WDL

DATE 11-19-63

9693A GS 48

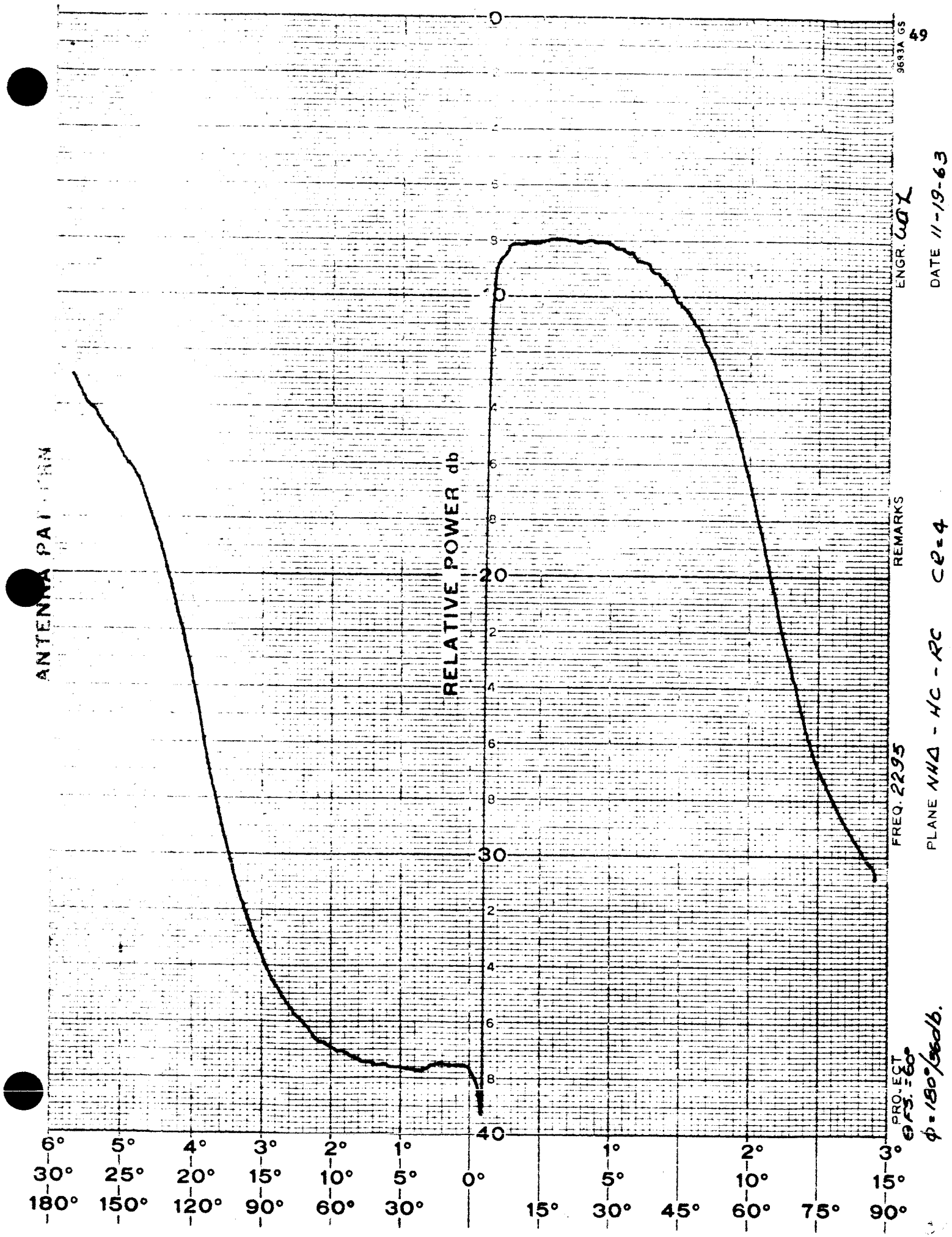

ANTENNA PATTERN
RELATIVE POWER db
0
10
20
30
40
6° 5° 4° 3° 2° 1° 1° 2° 3°
30° 25° 20° 15° 10° 5° 0° 5° 10° 15°
180° 150° 120° 90° 60° 30° 15° 30° 45° 60° 75° 90°
9693A GS
49
ENGR. WAL
DATE 11-19-63
REMARKS
FREQ. 2295
PLANE NHΔ - HC - RC CR=4
PROJECT
θ FS. = 60°
φ = 180°/36db.

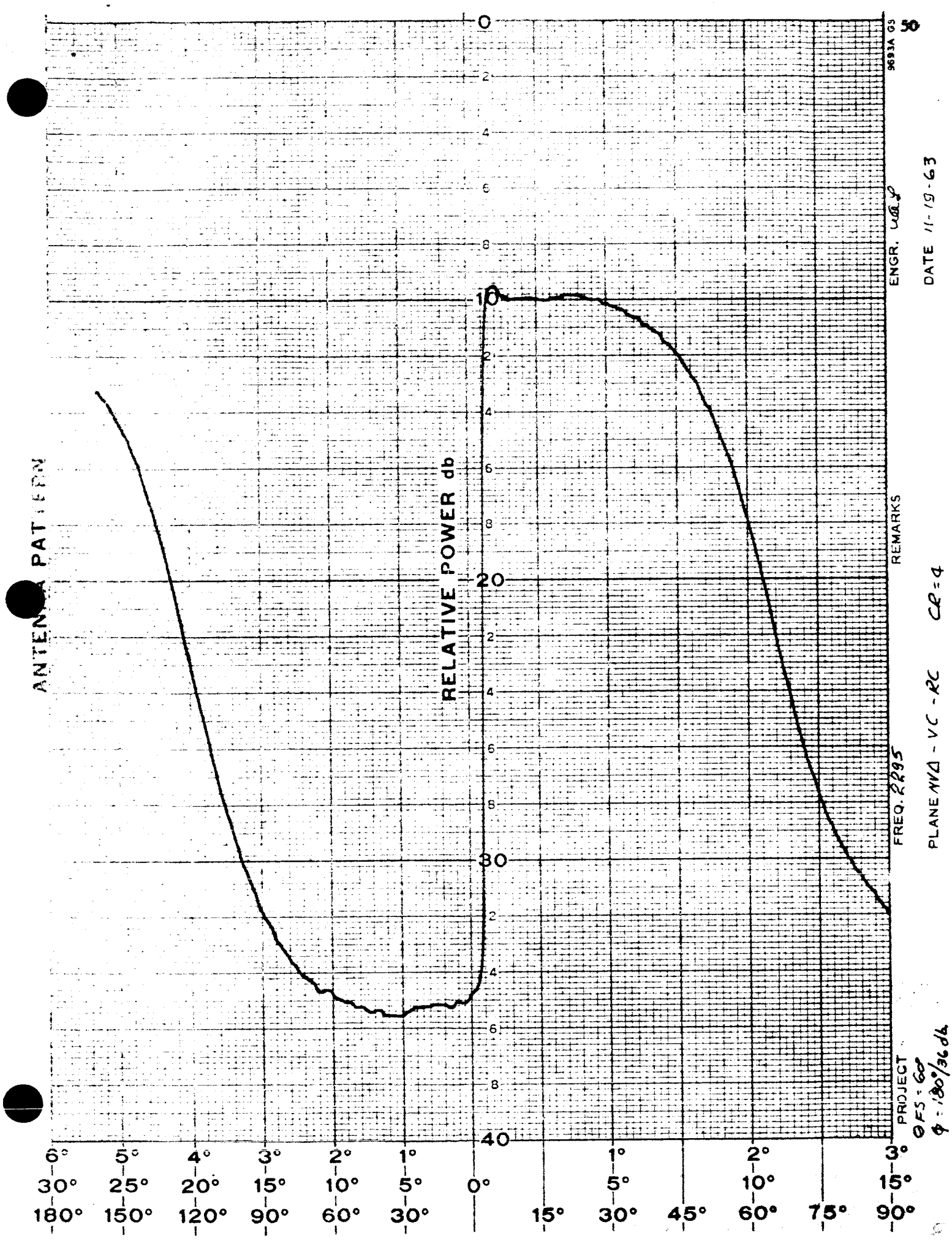
ANTENNA PATTERN
RELATIVE POWER db
0
2
4
6
8
10
20
30
40
6° 5° 4° 3° 2° 1° 1° 2° 3°
30° 25° 20° 15° 10° 5° 0° 5° 10° 15°
180° 150° 120° 90° 60° 30° 15° 30° 45° 60° 75° 90°
9693A G3
50
ENGR.
DATE 11-19-63
REMARKS
FREQ. 2295
PLANE NVΔ - VC - RC
CR=4
PROJECT
θFS: 60°
φ: 180°/36 db

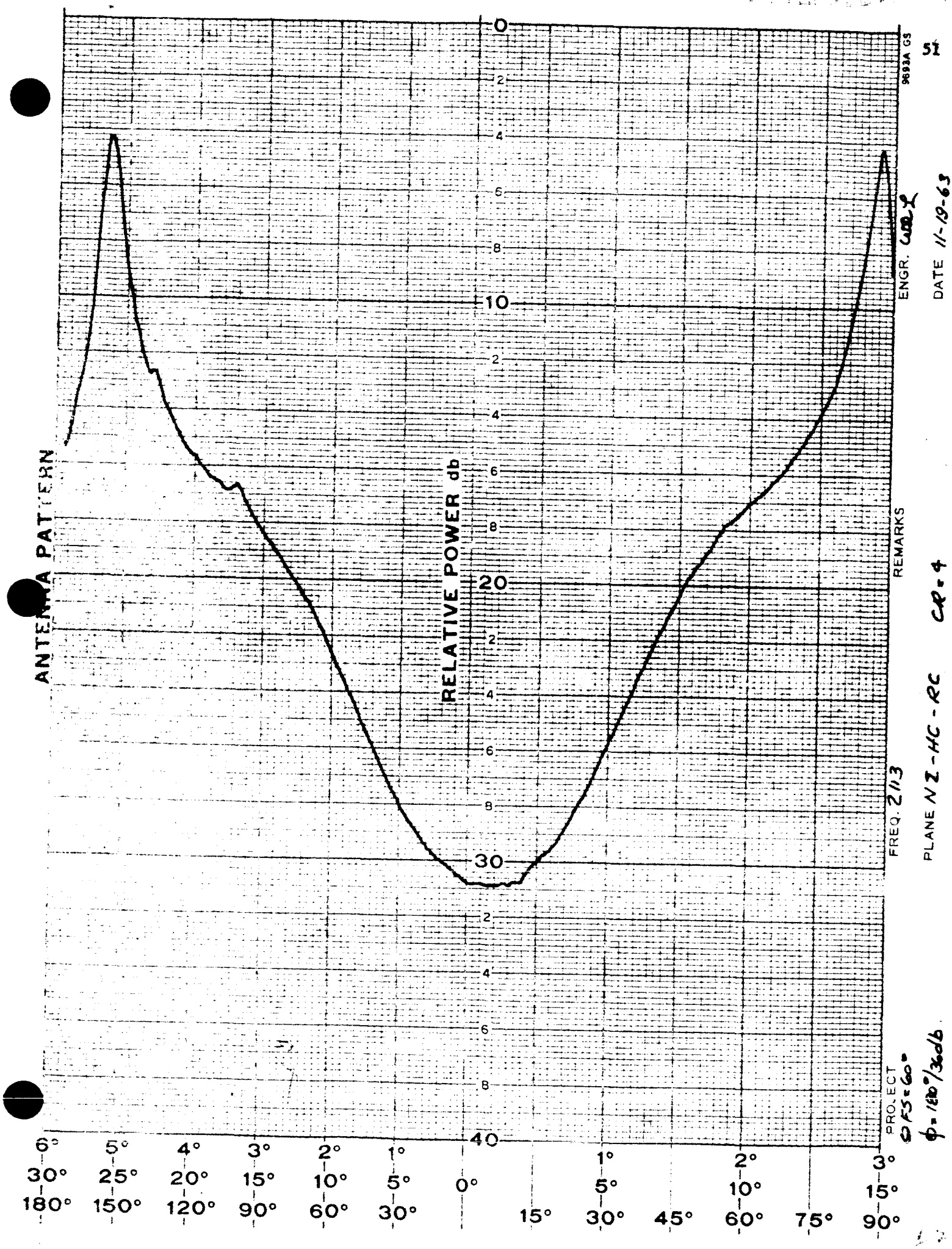

ANTENNA PATTERN
RELATIVE POWER db
0
2
4
6
8
10
20
30
40
6° 5° 4° 3° 2° 1° 1° 2° 3°
30° 25° 20° 15° 10° 5° 0° 5° 10° 15°
180° 150° 120° 90° 60° 30° 15° 30° 45° 60° 75° 90°
9693A GS
ENGR.
DATE 11-19-63
REMARKS
CR=4
FREQ. 2113
PLANE NZ-HC-RC
PROJECT
OFS=60°
φ=180°/36db

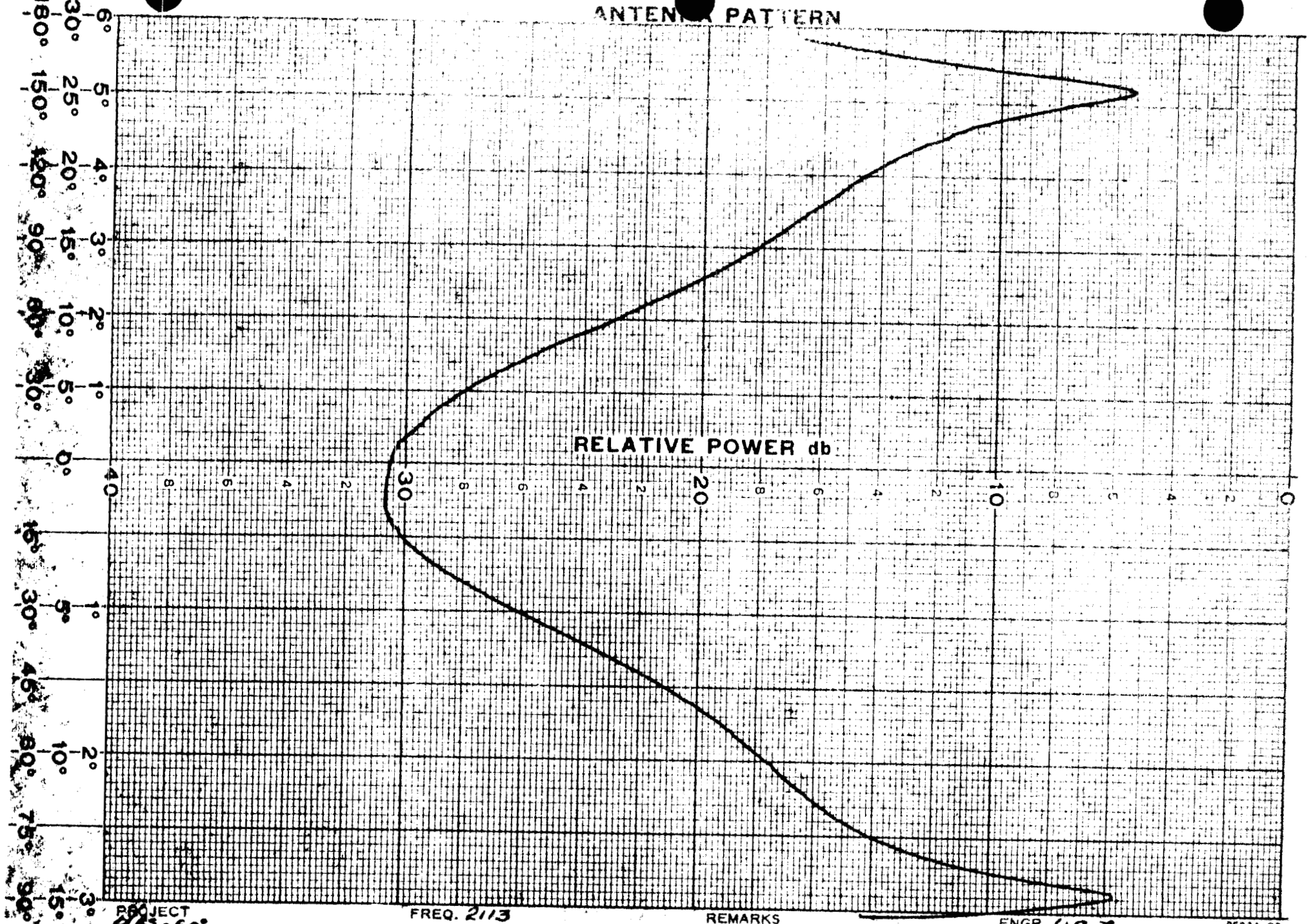

PROJECT
$\theta_{3} = 60°$
ϕ - 180/36db.

FREQ. 2113

REMARKS

ENGR. Ua I

9693A GS

PLANE NZ - VC - RC CR = 4

DATE 11-19-63

52
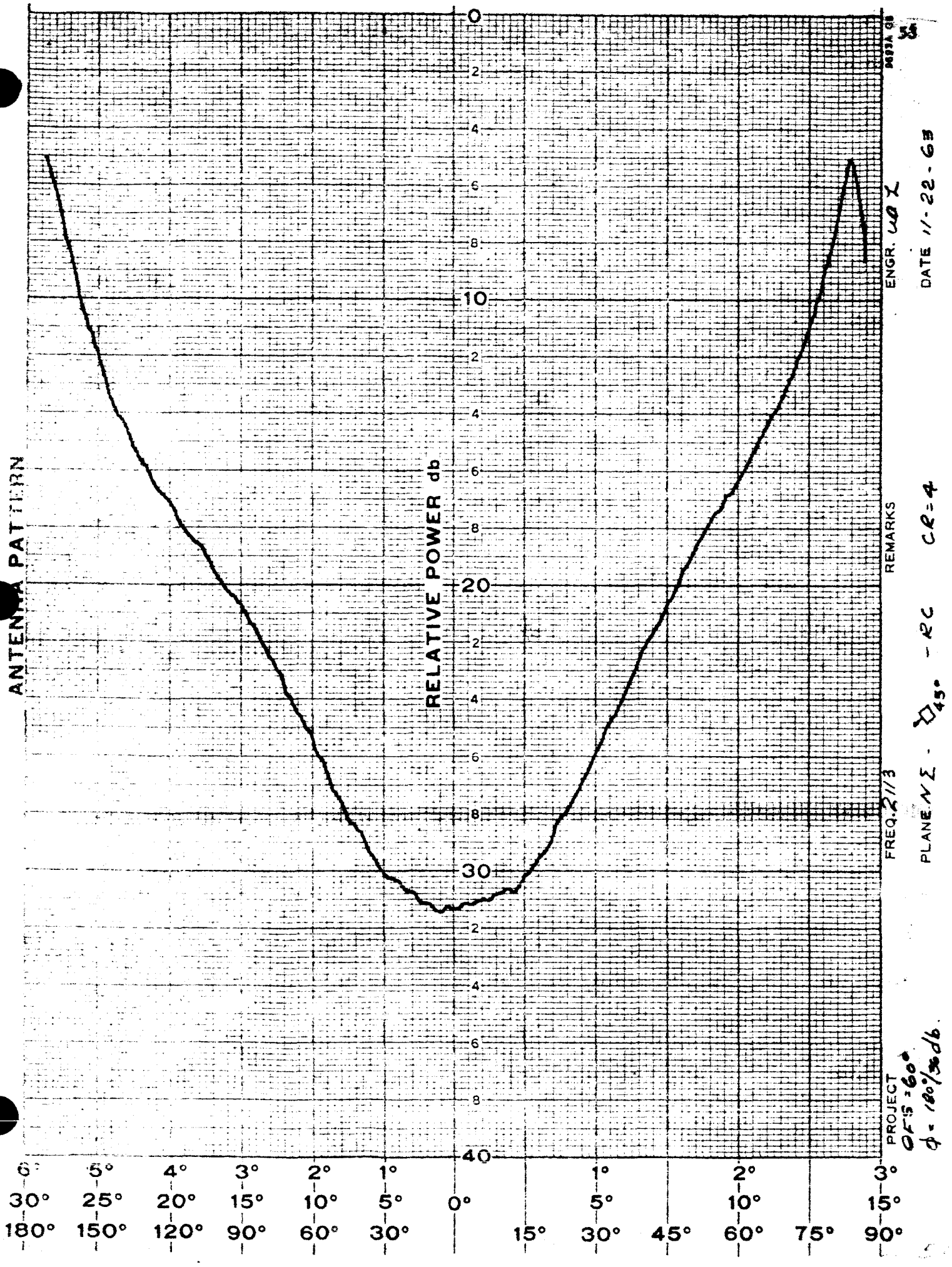
RE ORDER No. 64-52